Available online at www.sciencedirect.com
ScienceDirect
Lithos 99 (2007) 85–104
LITHOS
www.elsevier.com/locate/lithos

# Evidence for multi-stage metasomatism of chlorite-amphibole peridotites (Ulten Zone, Italy): Constraints from trace element compositions of hydrous phases

Marta Marocchi [a,*], Jörg Hermann [b], Lauro Morten [a,✠]

[a] *Dipartimento di Scienze della Terra e Geologico Ambientali, Bologna, Italy*
[b] *Research School of Earth Sciences, The Australian National University, Canberra, ACT, 0200, Australia*

Received 19 May 2006; accepted 15 May 2007
Available online 13 June 2007

**Abstract**

Peridotites from the Ulten Zone (Upper Austroalpine Domain, Central-Eastern Alps, Italy) derive from a mantle wedge environment and record a complex metamorphic history. This study focuses on amphibole–spinel peridotites and chlorite–tremolite peridotites. Chlorite is generally closely intergrown with Cr–spinel, indicating that it grew at the expense of former Al–spinel. No garnet relics or chlorite pseudomorphs after garnet have been found. Moreover, amphibole and chlorite trace element patterns display no fractionation in HREE, suggesting that these chlorite peridotites never equilibrated in the garnet stability field.

On the basis of textures, bulk rock and mineral major and trace element compositions three stages of metasomatism are documented in the mantle rocks. We propose that the earliest stage represents melt impregnation at plagioclase peridotite conditions and is unrelated to subduction. The metasomatism leading to spinel– and chlorite–amphibole peridotites is related to the progressive influx of a fluid with crustal signature, derived from neighbouring subducted continental crust as the mantle wedge peridotites approach the slab. The observation that garnet peridotites and chlorite peridotites, which never equilibrated in the garnet stability field, are hosted within the same gneisses, suggests that slices of mantle wedge peridotite with different *P-T* trajectories can be sampled by subducted and exhumed crust.


*Keywords:* Chlorite peridotites; Chlorite; Amphibole; Trace elements; Metasomatism; Ulten Zone

## 1. Introduction

Peridotite boudins enclosed within crustal rocks provide an excellent natural laboratory to study fluid-mediated element transfer in a crust–mantle system at great depth. Of particular interest are garnet peridotites, as a minimum pressure of 1.5 GPa is required to stabilize garnet in lherzolitic compositions (O'Neill, 1981; Robinson and Wood, 1998; Klemme and O'Neill, 2000). The incorporation of garnet peridotites in crustal rocks is a complex problem that is far from being fully understood. Two principal models have been proposed for the incorporation of garnet peridotites in orogenic belts: 1) subduction of oceanic or exhumed subcontinental

* Corresponding author. Dipartimento di Scienze della Terra e Geologico Ambientali, Università di Bologna, P.zza di P.ta S. Donato, 1, 40126, Bologna, Italy. Tel.: +39 051 2094956; fax: +39 051 2094904.
*E-mail address:* marta.marocchi@unibo.it (M. Marocchi).
✠ Deceased.

0024-4937/$ - see front matter © 2007 Elsevier B.V. All rights reserved.
doi:10.1016/j.lithos.2007.05.010

mantle into the garnet peridotite field. Such garnet peridotites often display clear evidence of a prograde metamorphic evolution and are associated with rocks such as rodingites, which clearly formed at shallow conditions (Evans and Trommsdorff, 1978; Trommsdorff et al., 2000); 2) sampling of mantle wedge peridotites by subducted crust followed by exhumation of both. These garnet peridotites preserve evidence of a high-temperature mantle evolution prior to their incorporation into the crust (Brueckner, 1998; Brueckner and Medaris, 2000; Nimis and Morten, 2000). Generally, the country rock gneisses of garnet peridotite lenses do not provide unambiguous evidence for ultra-high pressure metamorphism and hence it is not clear where the peridotites were assembled with the crust.

The Ulten Zone peridotites are one of the best examples of trapped slices of mantle wedge peridotite within continental crust (Morten and Obata, 1990; Nimis and Morten, 2000; Rampone and Morten, 2001; Tumiati et al., 2003; Marocchi et al., 2005; Marocchi, 2006; Scambelluri et al., 2006). In the Ulten Zone numerous small lens-shaped peridotitic bodies are included within high-grade garnet–kyanite gneisses and migmatite basement rocks belonging to the Upper Austroalpine domain (Tonale Nappe). The peridotites represent a portion of the Adria subcontinental mantle wedge, which underwent metasomatic enrichments (i.e. C–O–H fluid influx) during the subduction and likely during the late exhumation of a crustal slab. Seven mineral associations have been described (Morten, 1993; Morten and Trommsdorff, 2003) and related to a complex metamorphic *P*-*T* evolution from high-*T* spinel peridotites to relatively low-*T* garnet peridotites. The transition from spinel peridotites ($P$=1.5 GPa, $T$=1200 °C) to garnet (±amphibole)-peridotites associated with an increase in pressure and concomitant cooling ($P$=2.7 GPa, $T$=850 °C) has been interpreted as the result of corner flow within the mantle wedge followed by the incorporation of peridotites in a downgoing continental slab (Nimis and Morten, 2000). Within such an evolution, the chlorite–amphibole-bearing peridotites were interpreted by Obata and Morten (1987) as retrogressed garnet peridotite and were as such related to the exhumation of the peridotites (Morten and Trommsdorff, 2003). We have attempted to test this hypothesis with in situ trace element analyses of porphyroblastic minerals.

The main aim of this paper is to investigate in detail the metasomatic imprints recorded in chlorite–amphibole peridotites from the Ulten Zone. Previous studies of trace element characteristics of bulk-rocks and of main mineral phases revealed that the Ulten peridotites underwent multi-stage metasomatic events. An early metasomatic event led to Light Rare Earth Elements (LREE) and some Large Ion Lithophile Element (LILE) enrichment in spinel peridotites and has been interpreted to reflect interaction of subduction related magmas with peridotites at temperatures of ~1200 °C (Scambelluri et al., 2006). Extensive metasomatism at much lower temperatures of ~850 °C but higher pressures of ~2.7 GPa is documented at the transition from anhydrous spinel peridotites to hydrous amphibole–garnet peridotites. This metasomatism is well documented in LILE and LREE enriched amphibole and has been interpreted to reflect the influx of an aqueous fluid related to subducted continental crust (Morten and Obata, 1990; Rampone and Morten, 2001; Scambelluri et al., 2006).

In this study we report bulk rock major and trace element compositions of chlorite–amphibole peridotites and compare them to garnet peridotites to evaluate whether or not these rocks derive from the same protolith and share a common history of metasomatism. In situ trace element patterns of chlorite and amphibole in these peridotites provide constraints on the composition of the fluid phase that was present during exhumation. We compare the trace element composition of such amphiboles with amphiboles formed in equilibrium with garnet, to evaluate whether or not significant changes in fluid composition took place during the retrograde evolution of the peridotites. Furthermore, we will discuss the importance of the new data to better constrain the incorporation of peridotites into the country rock gneisses.

## 2. Geological setting and sample location

The Ulten Zone (Tonale Nappe, Upper Austroalpine Domain) forms a NNE striking belt, which is about 12 km long and 2–3 km wide. It is bounded to the NW by the Val Clapa Line and to the SE by the Rumo Line (Morten et al., 1976) (Fig. 1). The Ulten Zone is made of massive and foliated garnet–kyanite-bearing granulitic gneisses, migmatites, orthogneisses including small pods of eclogitic metabasites and small bodies of peridotites (Obata and Morten, 1987; Godard et al., 1996). The area has been the subject of several tectono-stratigraphic and petrological works (Morten et al., 2004 and references therein); the reader is referred to the above review paper for a more thorough description.

Most of the peridotite outcrops are lens-shaped bodies (*boudins*) with the major axis generally at least three times as long as the minor one. The peridotitic bodies, a few to ten metres thick and a few tens to hundreds metres long, form a discontinuous horizon between the

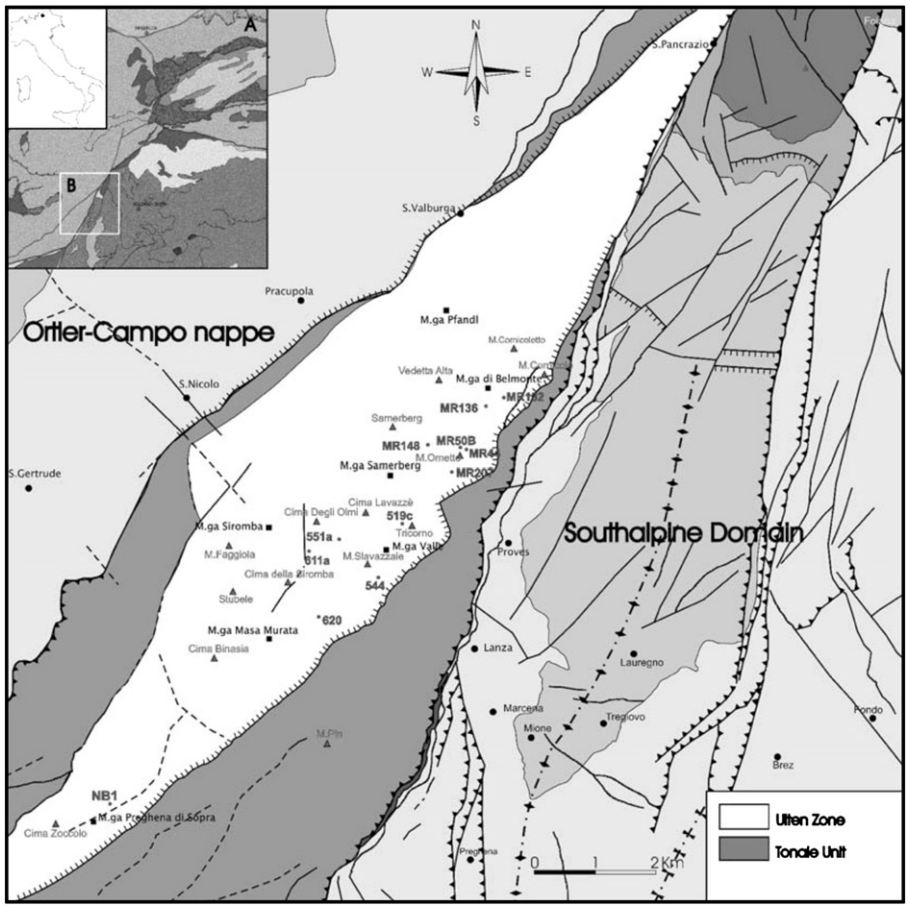


Fig. 1. Geological sketch map of the central-eastern Alps (A) and enlarged in (B) detailed geological map of the Ulten Zone with location of chlorite peridotite samples.

underlying garnet–kyanite gneisses (Fig. 2A) and the overlying migmatites and orthogneisses. Chlorite-bearing peridotites occur everywhere in the Ulten Zone terrane. Peridotites of this study have been sampled in the area between M. Ometto (*MandelSpitz*) and Buca di Cloz (*Clozner Loch*) and around M. Slavazzaie, M.ga Masa Murada and M.ga Preghena di Sopra (Fig. 1). The rocks are fine-grained and weakly to intensely deformed. The foliation is marked by the preferential orientation of amphibole, chlorite and opaque minerals. Shear zones with an intense foliation are common in the chlorite peridotites (Fig. 2B). The foliation is generally concordant with the main foliation of the country gneisses. Occasionally discordant chlorite veins occur in the chlorite peridotite lenses. The contact between the peridotitic bodies and the country rock gneisses is rarely exposed. In a few cases the contact zone is characterised by a narrow transition zone, consisting of phlogopite, talc, chlorite, anthophyllite and tremolite, which is partly overprinted by later serpentinization.

## 3. Petrography

Table 1 reports a summary of the mineral assemblages of 11 selected samples of chlorite peridotites. Obata and Morten (1987) classified the Ulten peridotites into two different textural types: coarse-type and fine-type. Chlorite-bearing peridotites display a tabular or mosaic equigranular texture (Fig. 3A) and belong to the "fine-type" group (Table 1). They consist of olivine, orthopyroxene, amphibole, chlorite and spinel relics included in chlorite porphyroblasts. Olivine is present as porphyroclast relics or as medium-sized crystals, sometimes arranged in mosaic polygonal textures. Orthopyroxene occurs either as smaller crystals or as porphyroclast relics in some of the samples, the latter often being kinked and fractured. The rocks have been strongly deformed, and widespread shear zones are characterised by the presence of secondary phases such as serpentine, opaque minerals and, in one case, talc. Two amphibole types are recognised: a pale-green,

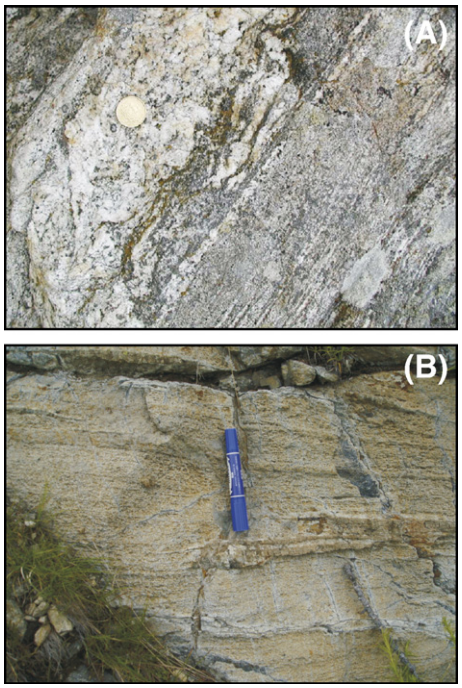


Fig. 2. (A) Outcrop photo of migmatic gneiss and (B) chlorite–peridotite showing a strong foliation.

euhedral calcic amphibole (Amph 1) and a late colourless and elongated tremolite (Amph 2). Calcic amphibole is euhedral and in textural equilibrium with olivine and orthopyroxene (Fig. 3B). Tremolite occurs as elongated crystals (Fig. 3C), often associated to chlorite to form aggregates. Occasionally, Amphibole 1 relics are preserved in the cores of tremolite.

Chlorite is always present in textural equilibrium with olivine, orthopyroxene and amphibole. Chlorite has been found in different textural sites, either as isolated and oriented crystals in the matrix or as medium-sized (3–4 mm) porphyroblasts with included spinel relics. Occasionally, chlorite forms flakes gathered in clusters together with amphibole and spinel (Fig. 3D, E, F). Chlorite generally occurs closely intergrown with Cr–spinel, indicating that it grew at the expense of former Al-rich spinel. No garnet relics or chlorite pseudomorphs after garnet have been found in the investigated samples.

## 4. Analytical techniques

Bulk rock major and trace element compositions were determined by ICP-MS at the "Centre de Recherches Petrographiques et Geochimiques" (CNRS, Nancy). Details on the analytical procedure can be found at www.crpg.cnrs-nancy.fr. Major element compositions were determined by ICP-AES and minor and trace element compositions by ICP-MS. Loss-on-ignition (L.O.I.) values were calculated after heating to 1000 °C.

Electron microprobe analyses (EMPA) were carried out at CNR (IGG-Geosciences and Georesources Institute), Padova, Italy, with a WDS (wavelength dispersive spectroscopy)-CAMECA-Camebax Microbeam 799 with four spectrometers WDS operating at 15 kV and 15 nA with a 10 s counting time both for major and minor elements. X-ray counts were converted into oxide weight percentage using a PAP correction program (Pouchou and Pichoir, 1984). Mineral trace elements were acquired in situ by laser ablation, inductively-coupled plasma mass spectrometry (LA ICP-MS) at the Research School of Earth Sciences (RSES), The Australian National University. The LA ICP-MS technique employs an ArF (193 nm) EXCIMER laser coupled

Table 1
Description of chlorite peridotite samples from the Ulten Zone

| Sample | Locality | Altitude | Texture | Petrography |
|---|---|---|---|---|
| 519c | Tricorno-Cima Lavazzè | 2200 a.s.l. | Porphyroclastic | ol+opx+amph+spl+chl+tlc |
| 544 | M. Slavazzaie | 2130 a.s.l. | Granoblastic | ol+opx+amph+spl+chl+serp |
| 551a | M. Slavazzaie | 2400 a.s.l. | Granoblastic | ol+opx+amph+sp+chl+serp |
| 611a | Passo Cemiglio | 2380 a.s.l. | Porphyroclastic | ol+opx+amph+spl+chl |
| 620 | Masa Murada | 1990 a.s.l. | Granoblastic | ol+opx+amph+spl+chl |
| MR44 | Monte Ometto | 2200 a.s.l. | Granoblastic | ol+opx+amph+spl+chl |
| MR50B | Monte Ometto | 2300 a.s.l. | Granoblastic | ol+opx+amph+spl+chl |
| MR132 | Buca di Cloz | 2150 a.s.l. | Granoblastic | ol+opx+amph+spl+chl+tlc+serp |
| MR136 | M.ga di Schongrübe | 2214 a.s.l. | Granoblastic | ol+opx+amph+spl+chl+tlc+serp |
| MR148 | Malga Samerberg | 2200 a.s.l. | Granoblastic | ol+opx+amph+spl+chl+serp |
| MR207 | Malga Samerberg | 2100 a.s.l. | Granoblastic | ol+opx+amph+spl+chl+tlc |
| NB1 | Malga Preghena di Sopra | 2084 a.s.l. | Granoblastic | ol+opx+amph+spl+chl+serp |

Mineral abbreviations after Kretz (1983).

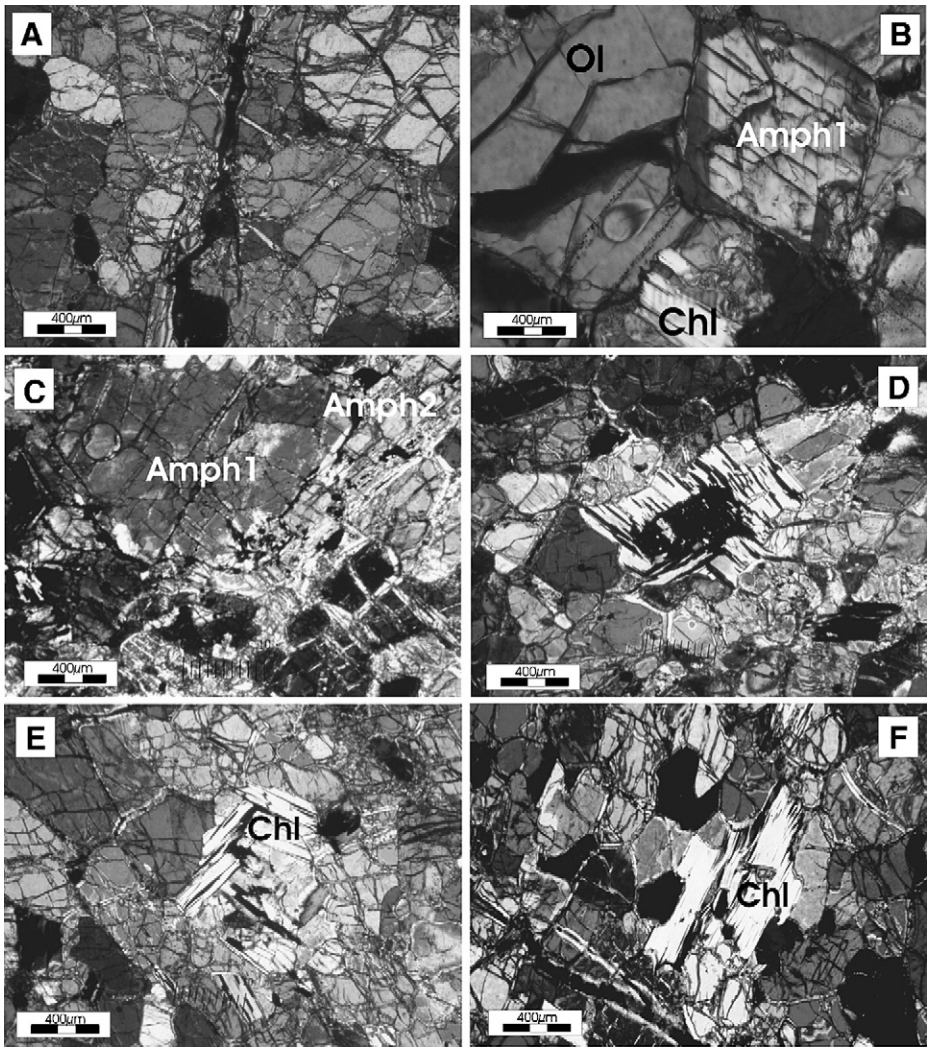


Fig. 3. Photomicrographs (transmitted cross-polarised light) of the Ulten Zone chlorite peridotites and representative rock forming minerals. (A) Mosaic equigranular texture with coarse olivine and orthopyroxene grains cut by shear zones, sample 519c. (B) Euhedral calcic amphibole (Amph1) in textural equilibrium with olivine and chlorite. (C) Photomicrograph showing amphibole textures: pargasite (Amph 1) is surrounded by elongated tremolite (Amph 2), sample MR207. Chlorite textural occurrences are: (D) porphyroblasts where chlorite replaces Cr–spinel, (E) flakes of chlorite forming clusters with spinel and amphibole and (F) oriented chlorite crystals scattered in the matrix. Length of bar 400 μm. Mineral abbreviations after Kretz (1983).

to an Agilent 7500 quadropole ICP-MS. A spot size of 187 μm was used and the counting time was 20 s for the background and between 40–45 s for sample analyses. $^{43}$Ca (for amphibole) and $^{29}$Si (for chlorite and orthopyroxene) were employed as the internal standard isotope, based on CaO and $SiO_2$ concentrations previously measured by electron microprobe. NIST-612 glass was used as the external standard, assuming the composition given by Pearce et al. (1997). A NIST 610 and BCR-2G glass was used as secondary standard. A detailed description of the technique is given in Buick et al. (2006).

## 5. Results

### 5.1. Bulk rock compositions

Whole-rock major and trace element compositions of the chlorite peridotites are listed in Table 2. The high L.O.I. values (from 1.6 to 6.83 wt.%) support the presence of hydrous phases in these samples (amphibole plus chlorite) and are directly correlated to their modal abundances. The peridotites display a variable range for some major elements, e. g. $Al_2O_3$ (1.7–2.87 wt.%) and MgO (38.9–43.28 wt.%).

Table 2
Bulk-rock major (wt.%) and trace (ppm) element compositions of chlorite–amphibole peridotites

| Sample | Group 1 | | | | | Group 2 | | | | | | |
|---|---|---|---|---|---|---|---|---|---|---|---|---|
| | 519c | 544 | 611a | 620 | MR44 | 551a | MR50B | MR132 | MR136A | MR148 | MR207 | NB1 |
| *Major elements (wt.%)* | | | | | | | | | | | | |
| $SiO_2$ | 43.03 | 42.26 | 43.22 | 43.63 | 42.92 | 41.93 | 43.19 | 42.35 | 42.2 | 42.27 | 42.05 | 41.78 |
| $Al_2O_3$ | 1.82 | 1.7 | 1.65 | 2.36 | 2.4 | 2.87 | 2.05 | 2.82 | 2.4 | 2.25 | 1.74 | 2.26 |
| $Fe_2O_3$* | 8.43 | 8.19 | 8.4 | 7.93 | 8.22 | 8.04 | 8.5 | 8.34 | 8.37 | 8.26 | 8.52 | 7.81 |
| MnO | 0.11 | 0.1 | 0.12 | 0.11 | 0.11 | 0.08 | 0.1 | 0.11 | 0.09 | 0.1 | 0.11 | 0.116 |
| MgO | 42.36 | 41.16 | 43.28 | 39.24 | 42.58 | 38.4 | 42.65 | 39.35 | 38.9 | 39.11 | 40.65 | 39.55 |
| CaO | 1.35 | 1.35 | 1.34 | 2.03 | 2.13 | 1.94 | 1.26 | 2.07 | 1.86 | 1.83 | 1.41 | 1.82 |
| $Na_2O$ | b.d.l | b.d.l. | b.d.l. | b.d.l. | b.d.l. | 0.16 | b.d.l. | b.d.l. | b.d.l. | b.d.l. | b.d.l. | 0.12 |
| K2O | b.d.l | b.d.l. | b.d.l. | b.d.l. | b.d.l. | b.d.l | b.d.l. | b.d.l. | b.d.l. | b.d.l. | b.d.l. | 0.06 |
| $TiO_2$ | b.d.l | b.d.l. | b.d.l. | b.d.l. | b.d.l. | 0.05 | b.d.l. | 0.07 | b.d.l. | b.d.l. | b.d.l. | 0.03 |
| $P_2O_5$ | 0.04 | 0.04 | 0.06 | 0.05 | b.d.l. | 0.06 | b.d.l. | b.d.l. | 0.05 | 0.06 | 0.05 | 0.01 |
| LOI | 2.52 | 5.16 | 1.6 | 4.45 | 1.84 | 6.5 | 2.49 | 4.95 | 5.6 | 4.74 | 5.39 | 6.83 |
| Total | 99.66 | 99.96 | 99.67 | 99.80 | 100.20 | 100.03 | 100.24 | 100.06 | 99.47 | 98.62 | 99.92 | 100.38 |
| *Trace elements (ppm)* | | | | | | | | | | | | |
| Rb | 2.5 | 1.4 | 1.0 | 2.0 | 1.7 | 2.4 | 1.5 | 1.9 | b.d.l. | 0.8 | 2.1 | 2.0 |
| Ba | 19 | 15 | 27 | 17 | 32 | 32 | 22 | 30 | 20 | 28 | 21 | 8 |
| Th | 0.23 | 0.19 | 0.23 | 0.26 | 0.27 | 0.29 | 0.34 | 0.12 | 0.21 | 0.36 | 0.36 | 0.22 |
| U | 0.08 | 0.11 | 0.09 | 0.10 | 0.12 | 0.14 | 0.12 | 0.08 | 0.13 | 0.17 | 0.16 | 0.08 |
| Nb | 0.23 | 0.22 | 0.23 | 0.45 | 0.27 | 0.54 | 0.80 | 0.47 | 0.33 | 0.33 | 0.60 | 0.50 |
| Ta | 0.04 | 0.01 | 0.03 | 0.05 | 0.02 | 0.03 | 0.09 | 0.03 | 0.02 | 0.02 | 0.04 | 0.01 |
| La | 0.79 | 0.98 | 1.05 | 1.79 | 1.60 | 1.01 | 1.31 | 0.87 | 0.75 | 1.49 | 1.13 | 1.37 |
| Ce | 1.96 | 1.86 | 2.16 | 3.71 | 3.19 | 2.44 | 3.52 | 2.48 | 2.07 | 3.40 | 3.09 | 2.00 |
| Pb | 1.29 | b.d.l. | 1.59 | 1.27 | 1.71 | b.d.l. | 2.58 | 1.56 | 2.27 | 1.63 | b.d.l. | b.d.l. |
| Pr | 0.23 | 0.19 | 0.24 | 0.37 | 0.33 | 0.33 | 0.48 | 0.36 | 0.29 | 0.41 | 0.41 | 0.17 |
| Sr | 8.5 | 9.5 | 17.0 | 16.9 | 12.9 | 10.0 | 14.1 | 10.4 | 7.7 | 14.6 | 10.4 | 16.0 |
| Nd | 0.78 | 0.64 | 0.84 | 1.14 | 1.12 | 1.43 | 2.03 | 1.54 | 1.21 | 1.59 | 1.65 | 0.51 |
| Zr | b.d.l. | b.d.l. | b.d.l. | 1.71 | 1.63 | 3.39 | 3.45 | 5.00 | 2.58 | 2.60 | 1.71 | 3.00 |
| Hf | b.d.l. | b.d.l. | b.d.l. | 0.05 | 0.05 | 0.11 | 0.10 | 0.16 | 0.08 | 0.07 | 0.04 | 0.09 |
| Sm | 0.12 | 0.11 | 0.15 | 0.15 | 0.15 | 0.38 | 0.39 | 0.33 | 0.26 | 0.30 | 0.31 | 0.09 |
| Eu | 0.05 | 0.04 | 0.05 | 0.06 | 0.06 | 0.09 | 0.08 | 0.16 | 0.08 | 0.09 | 0.08 | 0.04 |
| Gd | 0.10 | 0.09 | 0.12 | 0.11 | 0.12 | 0.35 | 0.30 | 0.33 | 0.28 | 0.25 | 0.24 | 0.13 |
| Tb | 0.02 | 0.02 | 0.02 | 0.02 | 0.02 | 0.06 | 0.04 | 0.05 | 0.05 | 0.04 | 0.04 | 0.02 |
| Ti | b.d.l. | b.d.l. | b.d.l. | b.d.l. | b.d.l. | 299 | b.d.l. | 419 | b.d.l. | b.d.l. | b.d.l. | 180 |
| Dy | 0.12 | 0.11 | 0.13 | 0.14 | 0.16 | 0.40 | 0.26 | 0.36 | 0.31 | 0.24 | 0.19 | 0.15 |
| Y | 0.77 | 0.68 | 0.68 | 0.90 | 1.06 | 2.29 | 1.52 | 2.07 | 1.82 | 1.48 | 1.18 | 0.90 |
| Ho | 0.03 | 0.03 | 0.02 | 0.03 | 0.04 | 0.08 | 0.05 | 0.08 | 0.07 | 0.06 | 0.04 | 0.03 |
| Er | 0.09 | 0.08 | 0.08 | 0.11 | 0.12 | 0.25 | 0.16 | 0.22 | 0.20 | 0.17 | 0.12 | 0.13 |
| Tm | 0.02 | 0.01 | 0.01 | 0.02 | 0.02 | 0.04 | 0.03 | 0.03 | 0.03 | 0.03 | 0.02 | 0.02 |
| Yb | 0.12 | 0.10 | 0.09 | 0.13 | 0.16 | 0.26 | 0.18 | 0.25 | 0.21 | 0.19 | 0.14 | 0.14 |
| Lu | 0.02 | 0.02 | 0.02 | 0.02 | 0.03 | 0.04 | 0.03 | 0.04 | 0.04 | 0.03 | 0.02 | 0.02 |
| Eu/Eu* | 0.18 | 0.17 | 0.29 | 0.27 | 0.28 | 2.08 | 1.83 | 1.74 | 1.17 | 1.15 | 1.20 | 0.21 |
| LaN/YbN | 2.24 | 0.80 | 1.39 | 2.63 | 0.81 | 0.57 | 2.17 | 0.55 | 0.49 | 0.62 | 1.06 | 0.50 |
| LaN/GdN | 6.88 | 9.05 | 7.55 | 14.08 | 11.69 | 2.54 | 3.83 | 2.30 | 2.29 | 5.29 | 4.03 | 9.14 |
| GdN/LuN | 0.61 | 0.68 | 1.00 | 0.57 | 0.57 | 0.99 | 1.31 | 1.05 | 1.00 | 0.92 | 1.44 | 0.60 |

* Total iron as $Fe_2O_3$.

Fig. 4 reports the variation of (a) $Al_2O_3$ wt.% and (b) MgO wt.% vs CaO wt.% for chlorite-peridotite samples, in relation to the compositions of Nonsberg peridotites compiled from the literature. It is important to note that the fields of chlorite peridotites overlap with the compositional range of garnet–amphibole and garnet-bearing peridotites.

The chemical trends are generally interpreted as normal trends of residua after variable degrees of partial melting and melt extraction (Bodinier and Godard, 2004). As outlined in previous works (Rampone and Morten, 2001), this major element variability is unrelated to the different textures but rather reflects pre-metamorphic heterogeneities, such as different degree of fertility of the

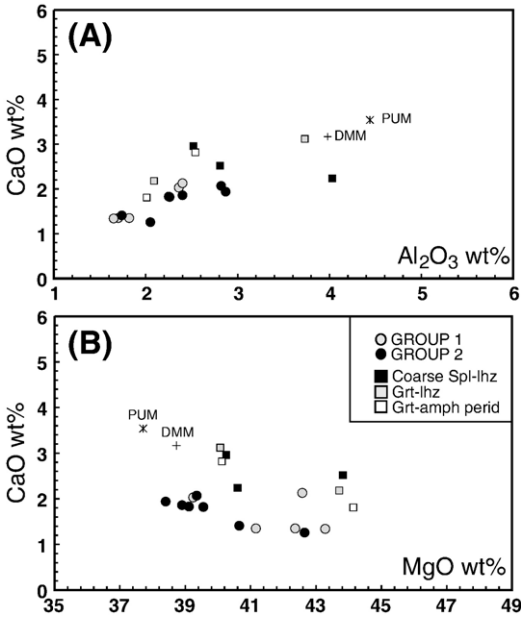


Fig. 4. Bulk-rock major element compositions (data from Table 2) of chlorite peridotites compared with Primitive Upper Mantle (PUM, McDonough and Sun, 1995), Depleted MORB Mantle (DMM, Workman and Hart, 2005) and peridotites from the Ulten Zone (data from Rampone and Morten, 2001, after Obata and Morten, 1987). Abbreviations: Spl-lhz=spinel-lherzolite, Grt-lhz=garnet-lherzolite, Grt–amph perid=garnet–amphibole peridotites.

mantle peridotite precursor. Chlorite peridotites plot along the general trend of depletion, starting from the estimated chemical compositions of the primitive upper mantle (PUM; McDonough and Sun, 1995) and of the depleted MORB mantle (DMM; Workman and Hart, 2005).

Chondrite-normalised (C1; Sun and McDonough, 1989) Rare Earth Element (REE) patterns are reported in Fig. 5A, while incompatible trace element spider diagrams normalised to the Primitive Mantle (PM; McDonough and Sun, 1995) are shown in Fig. 5B. Reference values of the depleted MORB mantle (DMM) and of the enriched DMM (EDMM) (Workman and Hart, 2005) have been reported for comparison. Chlorite peridotites have been grouped on the basis of main differences in REE patterns (cf. Table 2). Group 1 is characterised by a very steep decrease in Light (L)REE contents and Middle (M) REE contents below unity and a slight increase in Heavy (H)REE with increasing atomic number. Almost all samples display a moderate positive Eu anomaly. Group 2 displays higher MREE than Group 1 and a flat HREE pattern. Only one sample within this group displays a small positive Eu anomaly; all the others have either none or a small negative Eu anomaly. The HREE contents correlate with the degree of depletion of the peridotites: the samples of Group 1 (Fig. 5) are generally more depleted both in HREE and in CaO and $Al_2O_3$ (Fig. 4). Bulk-rock compositions of Spl-peridotites and Grt–Amph peridotites are reported from Scambelluri et al. (2006). It is worth noting that patterns of Group 2 chlorite peridotites are similar to those of Grt–Amph-peridotites (Fig. 5A), whereas Group 1 REE patterns are quite peculiar and have never been described before for the Ulten peridotites.

The PM-normalised trace element patterns are reported in Fig. 5B. The chlorite peridotites are characterised by a strong enrichment in LILE (between 1 and 10×PM) from Rb to U, and well-marked positive anomalies in U and Pb compared to the DMM (Fig. 5B). The LREE and LILE enrichment is generally unrelated to the depleted character of the sample in major components $Al_2O_3$ and CaO, but more likely due to a later addition of these elements to the peridotite system through an external agent. These features have been previously interpreted as the influx of a fluid derived from a crustal source (Rampone and Morten, 2001; Scambelluri et al., 2006).

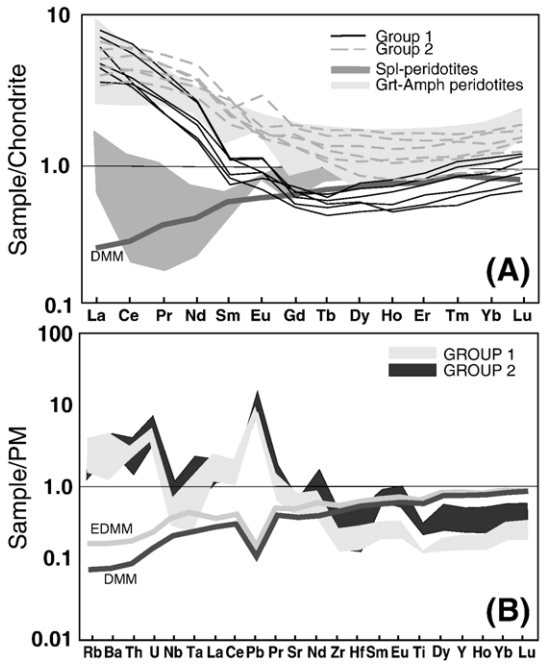


Fig. 5. Chondrite normalised REE (A) and Primitive Mantle (PM) normalised trace element (B) compositions of chlorite peridotite samples (data from Table 2). Shaded grey lines report compositions of Depleted MORB Mantle (DMM) and Enriched DMM (Workman and Hart, 2005). Group 1 and 2 refers to samples with positive and negative Eu anomaly respectively. Bulk-rock compositions of the Ulten Spl-peridotites and Grt-Amph-peridotites are reported from Scambelluri et al. (2006). Normalising values after Sun and McDonough (1989) for Chondrite and McDonough and Sun (1995) for PM.

Table 3
Representative major element compositions (wt.%) determined by Electron Microprobe

| Sample | 544 | | | | | 551a | | | | | MR136 | | | | | MR207 | | | | | | |
|---|---|---|---|---|---|---|---|---|---|---|---|---|---|---|---|---|---|---|---|---|---|---|
| Mineral | Ol | Opx | Amph1 | Amph2a | Chl | Ol | Opx | Amph1 | Amph2a | Chl | Ol | Opx | Amph1 | Amph2a | Chl | Ol | Opx | Amph1 | Amph2b | Chl | Spl | Spl |
| Location | Rim | Core | | | | Rim | Core | | | | Core | Core | | | | Core | Core | | | | In chl | Matrix |
| $SiO_2$ | 40.54 | 56.64 | 47.09 | 55.36 | 30.25 | 40.20 | 57.11 | 47.55 | 58.53 | 30.65 | 40.24 | 57.22 | 45.78 | 55.74 | 30.45 | 39.45 | 56.67 | 45.07 | 56.30 | 30.84 | 0.07 | 0.03 |
| $TiO_2$ | – | 0.26 | 0.25 | 0.07 | 0.03 | – | 0.12 | 0.19 | 0.03 | 0.00 | – | 0.05 | 0.36 | 0.11 | 0.02 | – | bdl | 0.55 | 0.09 | 0.04 | 0.24 | 0.06 |
| $Al_2O_3$ | – | 1.78 | 11.41 | 3.23 | 18.66 | – | 1.43 | 9.75 | 0.77 | 19.08 | – | 1.56 | 11.95 | 2.42 | 19.24 | – | 1.90 | 12.64 | 2.02 | 18.44 | 13.09 | 38.88 |
| $Cr_2O_3$ | – | 0.10 | 1.01 | 0.60 | 1.34 | – | 0.19 | 1.04 | 0.07 | 1.25 | – | 0.19 | 1.36 | 0.44 | 1.02 | – | 0.18 | 0.66 | 0.21 | 2.22 | 47.61 | 25.82 |
| FeOtot | 9.49 | 6.66 | 2.75 | 2.22 | 2.98 | 10.62 | 6.69 | 2.97 | 2.02 | 2.72 | 10.81 | 7.07 | 3.55 | 2.17 | 3.29 | 9.78 | 6.18 | 3.04 | 1.82 | 2.86 | 29.23 | 18.78 |
| MnO | 0.14 | 0.09 | 0.08 | 0.10 | 0.04 | 0.09 | 0.06 | 0.14 | 0.03 | 0.08 | 0.17 | 0.18 | 0.07 | 0.10 | bdl | 0.07 | 0.14 | 0.00 | 0.07 | 0.00 | 0.41 | 0.18 |
| MgO | 49.44 | 34.50 | 19.53 | 22.58 | 32.37 | 49.58 | 34.85 | 19.60 | 23.64 | 32.63 | 48.24 | 34.25 | 18.83 | 22.85 | 32.07 | 48.95 | 34.58 | 18.41 | 22.81 | 32.18 | 5.46 | 12.81 |
| CaO | 0.03 | 0.01 | 13.06 | 13.17 | 0.01 | 0.02 | 0.06 | 12.89 | 13.19 | 0.01 | 0.03 | 0.23 | 13.01 | 13.53 | 0.04 | 0.03 | 0.24 | 12.98 | 13.21 | 0.05 | 0.01 | 0.00 |
| $Na_2O$ | – | bdl | 1.96 | 0.58 | bdl | – | 0.03 | 1.62 | 0.08 | 0.03 | – | 0.00 | 2.25 | 0.41 | bdl | – | bdl | 2.25 | 0.39 | bdl | – | – |
| $K_2O$ | – | – | 0.73 | 0.11 | 0.02 | – | – | 0.52 | 0.04 | bdl | – | – | 0.19 | 0.07 | bdl | – | – | 0.37 | 0.10 | bdl | – | – |
| NiO | 0.35 | – | – | – | – | 0.34 | – | – | – | – | 0.25 | – | – | – | – | 0.35 | – | | | | | |
| Total | 100.00 | 100.00 | 97.88 | 98.00 | 85.69 | 100.85 | 100.60 | 96.26 | 98.38 | 86.45 | 99.74 | 100.70 | 97.35 | 97.83 | 86.14 | 98.64 | 99.90 | 95.97 | 97.02 | 86.62 | 96.14 | 96.57 |
| Si | 0.99 | 1.95 | 6.58 | 7.56 | 5.80 | 0.98 | 1.95 | 6.73 | 7.89 | 5.82 | 0.99 | 1.96 | 6.45 | 7.63 | 5.81 | 0.98 | 1.95 | 6.44 | 7.74 | 5.86 | 0.00 | 0.00 |
| $Al^{(iv)}$ | – | 0.05 | 1.42 | 0.44 | | – | 0.05 | 1.27 | 0.11 | | – | 0.04 | 1.55 | 0.37 | | – | 0.05 | 1.56 | 0.26 | | | |
| $Al^{(vi)}$ | – | 0.02 | 0.46 | 0.08 | 4.22† | – | 0.01 | 0.36 | 0.01 | 4.26† | – | 0.02 | 0.43 | 0.02 | 4.33† | – | 0.03 | 0.57 | 0.07 | 4.13† | 0.54† | 1.36† |
| Ti | – | 0.01 | 0.03 | 0.01 | 0.01 | – | 0.00 | 0.02 | 0.00 | 0.00 | – | 0.00 | 0.04 | 0.01 | 0.00 | – | bdl | 0.06 | 0.01 | 0.01 | 0.01 | 0.00 |
| Cr | – | 0.00 | 0.11 | 0.06 | 0.20 | – | 0.01 | 0.12 | 0.01 | 0.19 | – | 0.01 | 0.15 | 0.05 | 0.15 | – | 0.00 | 0.07 | 0.02 | 0.33 | 1.31 | 0.61 |
| $Fe^{3+}$ | | | | | | | | | | | | | | | | | | | | | 0.14 | 0.03 |
| $Fe^{2+}$ | 0.20 | 0.19* | 0.32 | 0.25 | 0.48* | 0.22 | 0.19* | 0.35 | 0.23 | 0.43* | 0.22 | 0.20* | 0.42 | 0.25 | 0.53* | 0.20 | 0.18* | 0.36 | 0.21 | 0.46* | 0.71 | 0.43 |
| Mn | 0.00 | 0.00 | 0.01 | 0.01 | 0.01 | 1.81 | 0.00 | 0.02 | 0.00 | 0.01 | 1.78 | 0.01 | 0.01 | 0.01 | bdl | 1.82 | 0.00 | 0.00 | 0.01 | 0.00 | 0.01 | 0.01 |
| Mg | 1.81 | 1.77 | 4.07 | 4.59 | 9.26 | 0.00 | 1.78 | 4.14 | 4.75 | 9.23 | 0.00 | 1.75 | 3.95 | 4.66 | 9.12 | 0.00 | 1.78 | 3.92 | 4.68 | 9.11 | 0.28 | 0.57 |
| Ca | 0.00 | 0.00 | 1.96 | 1.93 | 0.00 | 0.01 | 0.00 | 1.95 | 1.90 | bdl | 0.00 | 0.01 | 1.96 | 1.98 | 0.01 | 0.01 | 0.01 | 1.99 | 1.95 | 0.01 | 0.00 | 0.00 |
| Na | – | bdl | 0.53 | 0.15 | bdl | – | 0.00 | 0.44 | 0.02 | 0.01 | – | 0.00 | 0.61 | 0.11 | bdl | – | bdl | 0.62 | 0.11 | bdl | – | – |
| K | – | – | 0.13 | 0.02 | 0.01 | – | – | 0.09 | 0.01 | bdl | – | – | 0.03 | 0.01 | bdl | – | – | 0.07 | 0.02 | bdl | – | – |
| Cation sum | 3.00 | 4.00 | 15.62 | 15.10 | 19.98 | 3.02 | 4.00 | 15.49 | 14.94 | 19.96 | 3.00 | 4.00 | 15.61 | 15.11 | 19.95 | 3.00 | 4.00 | 15.67 | 15.06 | 19.90 | 3.00 | 3.00 |

The structural formula of olivine was calculated on the basis of 4 oxygens. Orthopyroxenes are normalised on the basis of 4 cations and 6 oxygens. Calcic amphiboles are normalised on the basis of 23 oxygens with all Fe as $Fe^{2+}$. Chlorites are normalised on the basis of 28 oxygens. All Fe was assumed to be $Fe^{2+}$ for olivine and chlorite. †=total aluminum as $Al^{VI}$; *=total iron as $Fe^{2+}$. Mineral abbreviations as in Table 1. *bdl*=below detection limit.

### 5.2. Major element mineral compositions

Selected microprobe analyses of olivine, orthopyroxene, amphibole, chlorite and spinel are reported in Table 3.

*Olivine* is generally unzoned and homogeneous in composition (Fo% 88–90). Olivine compositions in chlorite peridotites are comparable to those of other Nonsberg peridotites (Fo% ranging from 89.4 to 90.5, Obata and Morten, 1987) but the former have generally higher NiO contents (i.e. 0.35–0.40 vs 0.22–0.25). *Orthopyroxene* (Mg# 0.88–0.90) shows relatively homogeneous composition either in the porphyroclasts relics, when present, or in the smaller orthopyroxene crystals. Coarse orthopyroxene grains are more aluminous than the smaller ones in the same sample (e.g. 1.29–2.18 vs 0.73–2.02 $Al_2O_3$ wt.%) and they generally have slight zonation patterns for Al, Cr and Ca. In particular, Al content is highest in the core of porphyroclasts (up to 2.18 $Al_2O_3$ wt.%). *Chlorite* composition is uniform, regardless of its textural position. Chlorite is mostly clinochlore with a high $Cr_2O_3$ content ($Cr_2O_3$ 1.35–1.84), with the exception of a few samples in which chlorite contains Si > 6.2 atoms per formula unit (a.p.f.u.) and is thus classified as penninite. Interstitial *spinel* or spinel associated to amphibole is Al-rich and Cr-poor (Cr/(Cr+Al)=0.25–0.50) when compared to spinel within chlorite porphyroclasts, which displays higher values (Cr/(Cr+Al)= 0.65–0.75). Two different generations of *amphibole* (Amph 1 and Amph 2) have been detected. Amphibole major element compositions are plotted in terms of atoms per formula unit (a.p.f.u.) for Si vs Cr and Ti (Fig. 6). According to the classification of Leake et al. (1997), the first amphibole compositionally ranges from Mg-hornblende, edenitic-hornblende or pargasitic-hornblende cores to mainly edenite at rims (Si=6.3–6.9 cations per 23 oxygens formula unit). The second amphibole is generally unzoned and has tremolite composition (Si=7.1–7.8 cations per 23 oxygens formula unit). The pargasitic-hornblende contains significant Cr and Al (up to 1.57 wt.% $Cr_2O_3$) (Table 3).

The *Si-content* per formula unit of amphibole appears to be the compositional parameter most sensitive to metamorphic grade, producing a continuous trend from tremolite, through tremolitic hornblende, Mg-hornblende and pargasitic hornblende, to pargasite (Fig. 6). Amphiboles from Nonsberg garnet–amphibole peridotites (Obata and Morten, 1987; Rampone and Morten, 2001) are reported for comparison: they are pargasites, which generally display higher Cr and Ti contents if compared to pargasites from chlorite-bearing peridotites (Fig. 6).

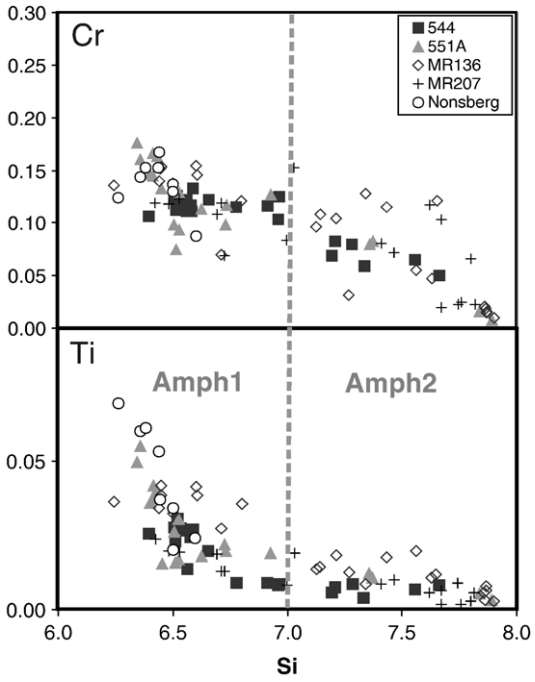


Fig. 6. Plot of Si vs Cr and Ti (atoms per formula unit) for amphiboles of samples 544, 551A, MR136, MR207. Amphibole compositions from Nonsberg garnet–amphibole peridotites are reported for comparison (data from Rampone and Morten, 2001).

### 5.3. LA ICP-MS: trace element mineral compositions

Sample selection for LA ICP-MS analyses was done on the basis of textural characters and whole-rock major element compositions. We selected samples 551A-MR136 and samples 544-MR207 representative of the more fertile and depleted chlorite peridotites respectively (Fig. 4) and covering all the chlorite textural occurrences. Mineral analyses acquired by in situ LA ICP-MS for the chlorite peridotite samples are reported in Tables 4 and 5 and shown in Fig. 7.

Textural observations combined with electron microprobe analyses have shown that the hornblende (Amph1) and the tremolite (Amph 2) are often intergrown. These two amphiboles show distinct $TiO_2$ and $Al_2O_3$ contents (Table 3) and we have used Ti and Al contents measured with the LA ICP-MS to relate trace element patterns to the two amphibole generations. Amphiboles from all samples are generally characterised by spoon-shaped REE patterns, with a variable degree of enrichment in LREE compared to MREE ($La_N/Gd_N$=1.18–10.88). Amphibole 1 is characterised by enrichment in LREE and by a large LREE/HREE fractionation (Fig. 7A). The full trace element pattern normalised to primitive mantle displays a high LILE content with characteristic $Ba_N > Rb_N$ and

Table 4
Trace element compositions (ppm) of amphibole determined with LA-ICP-MS

| Sample | 544 | | | 551a | | | | | MR136 | | | | | | | MR207 | | | |
|---|---|---|---|---|---|---|---|---|---|---|---|---|---|---|---|---|---|---|---|
| Amph type | Amph 1 | Amph 2a | Amph 2a | Amph 1 | Amph 1 | Amph 1 | Amph 1 | Amph 2a | Amph 1 | Amph 1 | Amph 1 | Amph 1 | Amph 1 | Amph 2a | Amph 2a | Amph 1 | Amph 2b | Amph 2b | Amph 2b |
| Li | 0.73 | 0.40 | 1.33 | 1.67 | 1.79 | 2.14 | 2.02 | 1.52 | 0.38 | 0.85 | 0.20 | 0.46 | 0.16 | 0.10 | 0.23 | 2.80 | 2.94 | 1.21 | 1.57 |
| Be | 0.71 | 0.31 | 0.37 | 1.32 | 1.30 | 1.44 | 1.52 | 0.62 | 1.23 | 1.05 | 1.25 | 1.39 | 0.78 | 0.41 | 0.33 | 1.88 | 0.84 | 0.99 | 1.15 |
| Cs | 0.12 | 0.14 | 0.38 | 1.93 | 0.50 | 0.78 | 0.58 | 0.19 | 0.18 | 0.19 | 0.35 | 0.36 | 0.28 | 0.08 | 0.03 | 0.45 | 0.19 | 0.17 | 0.17 |
| Rb | 16.65 | 3.09 | 5.56 | 10.97 | 17.02 | 16.35 | 24.23 | 3.90 | 4.92 | 3.50 | 5.79 | 5.88 | 3.89 | 1.27 | 0.69 | 20.77 | 2.44 | 1.50 | 4.77 |
| Ba | 331 | 21 | 49 | 402 | 711 | 505 | 592 | 30 | 520 | 240 | 630 | 643 | 320 | 33 | 8 | 802 | 20 | 16 | 59 |
| Pb | 14.28 | 0.98 | 2.37 | 2.11 | 8.30 | 3.28 | 3.05 | 1.08 | 4.74 | 2.30 | 3.45 | 5.79 | 3.58 | 2.91 | 0.88 | 13.53 | 0.89 | 1.33 | 1.42 |
| Th | 1.51 | 0.68 | 0.78 | 1.24 | 1.90 | 1.64 | 1.65 | 0.77 | 0.88 | 0.82 | 1.01 | 1.12 | 0.69 | 0.36 | 0.30 | 0.86 | 0.54 | 0.71 | 0.81 |
| U | 1.11 | 0.37 | 0.37 | 0.53 | 0.77 | 0.65 | 0.67 | 0.27 | 0.37 | 0.33 | 0.43 | 0.46 | 0.27 | 0.10 | 0.10 | 0.95 | 0.14 | 0.22 | 0.23 |
| Nb | 3.54 | 0.81 | 1.12 | 4.08 | 6.43 | 5.06 | 5.65 | 1.63 | 4.71 | 2.73 | 4.39 | 5.18 | 3.21 | 1.14 | 0.83 | 14.02 | 3.11 | 3.60 | 4.09 |
| Ta | 0.21 | 0.03 | 0.06 | 0.20 | 0.36 | 0.27 | 0.32 | 0.07 | 0.21 | 0.13 | 0.21 | 0.24 | 0.16 | 0.05 | 0.04 | 0.64 | 0.16 | 0.21 | 0.18 |
| P | 30.82 | 27.31 | 30.19 | 81.4 | 107.6 | 81.7 | 115.5 | 34.8 | 79.0 | 66.5 | 84.3 | 87.4 | 54.6 | 30.9 | 27.5 | 79.3 | 47.6 | 40.3 | 36.9 |
| La | 13.79 | 4.34 | 5.90 | 5.69 | 13.09 | 8.92 | 9.90 | 2.09 | 10.75 | 6.23 | 10.65 | 11.72 | 7.57 | 2.67 | 2.02 | 17.87 | 6.44 | 7.70 | 8.39 |
| Ce | 24.84 | 8.19 | 11.90 | 15.76 | 23.92 | 19.28 | 21.01 | 6.63 | 26.10 | 16.43 | 25.60 | 28.33 | 19.32 | 9.36 | 6.73 | 52.31 | 20.59 | 25.41 | 25.82 |
| Pr | 2.64 | 0.78 | 1.21 | 2.32 | 2.84 | 2.44 | 2.63 | 1.03 | 3.32 | 2.15 | 3.21 | 3.56 | 2.56 | 1.41 | 1.03 | 7.02 | 2.80 | 3.60 | 3.57 |
| Sr | 216.5 | 40.8 | 57.7 | 81.1 | 164.0 | 115.6 | 130.0 | 34.8 | 149.2 | 76.3 | 150.9 | 175.2 | 94.6 | 22.2 | 22.2 | 372.1 | 25.4 | 37.7 | 53.6 |
| Nd | 9.53 | 2.49 | 4.19 | 10.74 | 11.83 | 10.66 | 11.00 | 5.00 | 13.60 | 8.96 | 13.11 | 14.52 | 10.88 | 6.38 | 4.85 | 29.14 | 11.92 | 15.60 | 15.37 |
| Zr | 10.86 | 2.96 | 4.14 | 20.48 | 24.78 | 21.91 | 22.96 | 9.62 | 15.92 | 12.99 | 17.06 | 18.43 | 12.33 | 6.46 | 5.95 | 16.32 | 8.24 | 9.70 | 10.20 |
| Hf | 0.37 | 0.09 | 0.16 | 0.74 | 1.27 | 0.97 | 1.00 | 0.28 | 0.60 | 0.42 | 0.63 | 0.66 | 0.48 | 0.20 | 0.19 | 0.51 | 0.22 | 0.30 | 0.26 |
| Sm | 1.50 | 0.35 | 0.64 | 2.47 | 2.31 | 2.27 | 2.28 | 1.35 | 2.37 | 1.79 | 2.33 | 2.58 | 2.16 | 1.48 | 1.24 | 4.36 | 2.42 | 3.00 | 3.14 |
| Eu | 0.43 | 0.17 | 0.24 | 0.73 | 0.64 | 0.65 | 0.63 | 0.37 | 0.72 | 0.63 | 0.70 | 0.76 | 0.64 | 0.53 | 0.41 | 0.98 | 0.57 | 0.79 | 0.80 |
| Ti | 1811 | 684 | 773 | 2237 | 3333 | 2880 | 3343 | 1165 | 2453 | 1985 | 2296 | 2782 | 1967 | 1127 | 852 | 1495 | 575 | 699 | 781 |
| Gd | 1.37 | 0.35 | 0.61 | 2.48 | 2.13 | 2.14 | 2.17 | 1.48 | 2.07 | 1.92 | 2.12 | 2.29 | 2.20 | 1.78 | 1.49 | 2.66 | 2.02 | 2.45 | 2.75 |
| Tb | 0.20 | 0.06 | 0.09 | 0.40 | 0.27 | 0.32 | 0.30 | 0.26 | 0.30 | 0.32 | 0.31 | 0.34 | 0.35 | 0.30 | 0.26 | 0.30 | 0.28 | 0.34 | 0.40 |
| Dy | 1.42 | 0.43 | 0.72 | 2.75 | 1.68 | 2.03 | 1.81 | 1.90 | 1.89 | 2.34 | 2.06 | 2.14 | 2.34 | 2.17 | 1.88 | 1.70 | 1.83 | 2.13 | 2.72 |
| Ho | 0.30 | 0.10 | 0.17 | 0.60 | 0.30 | 0.41 | 0.33 | 0.43 | 0.38 | 0.51 | 0.41 | 0.43 | 0.48 | 0.48 | 0.42 | 0.31 | 0.37 | 0.43 | 0.56 |
| Y | 7.83 | 2.81 | 4.39 | 15.72 | 7.61 | 10.67 | 8.73 | 11.22 | 9.88 | 13.75 | 10.82 | 11.05 | 12.12 | 12.43 | 10.74 | 8.29 | 9.89 | 11.48 | 14.90 |
| Er | 0.91 | 0.37 | 0.55 | 1.92 | 0.82 | 1.26 | 0.93 | 1.39 | 1.13 | 1.68 | 1.26 | 1.27 | 1.38 | 1.52 | 1.28 | 0.88 | 1.12 | 1.31 | 1.75 |
| Tm | 0.14 | 0.06 | 0.09 | 0.29 | 0.11 | 0.19 | 0.14 | 0.22 | 0.17 | 0.27 | 0.19 | 0.20 | 0.20 | 0.23 | 0.19 | 0.12 | 0.17 | 0.20 | 0.26 |
| Yb | 1.00 | 0.51 | 0.69 | 2.16 | 0.77 | 1.34 | 1.01 | 1.51 | 1.27 | 2.00 | 1.51 | 1.43 | 1.46 | 1.60 | 1.30 | 0.87 | 1.24 | 1.46 | 1.87 |
| Lu | 0.15 | 0.09 | 0.12 | 0.34 | 0.12 | 0.22 | 0.16 | 0.23 | 0.20 | 0.32 | 0.24 | 0.23 | 0.22 | 0.24 | 0.19 | 0.13 | 0.19 | 0.21 | 0.28 |
| Sc | 92.1 | 55.0 | 63.4 | 83.1 | 52.9 | 61.8 | 51.8 | 62.2 | 56.6 | 77.7 | 65.4 | 64.8 | 64.1 | 70.0 | 54.0 | 91.6 | 58.6 | 78.4 | 90.8 |
| Th/U | 1.36 | 1.84 | 2.09 | 2.35 | 2.46 | 2.52 | 2.47 | 2.81 | 2.39 | 2.48 | 2.35 | 2.46 | 2.58 | 3.67 | 2.99 | 0.90 | 3.95 | 3.17 | 3.53 |
| Rb/Ba | 0.05 | 0.15 | 0.11 | 0.03 | 0.02 | 0.03 | 0.04 | 0.13 | 0.01 | 0.01 | 0.01 | 0.01 | 0.01 | 0.04 | 0.08 | 0.03 | 0.12 | 0.09 | 0.08 |
| $La_N/Gd_N$ | 8.70 | 10.88 | 8.38 | 1.99 | 5.34 | 3.61 | 3.95 | 1.23 | 4.49 | 2.82 | 4.35 | 4.44 | 2.98 | 1.30 | 1.18 | 5.83 | 2.77 | 2.72 | 2.65 |
| $Gd_N/Lu_N$ | 1.11 | 0.47 | 0.65 | 0.90 | 2.26 | 1.20 | 1.67 | 0.79 | 1.26 | 0.73 | 1.10 | 1.25 | 1.21 | 0.92 | 0.96 | 2.61 | 1.29 | 1.43 | 1.21 |

Amph type refers to different amphibole generations.

Table 5
Trace element compositions (ppm) of chlorite, orthopyroxene and olivine determined with LA-ICP-MS

| Sample | 544 | 551a | | MR136 | | MR207 | | | | |
|---|---|---|---|---|---|---|---|---|---|---|
| Mineral | Ol (4) | Ol (2) | Chl (3) | Ol (5) | Chl | Ol (2) | Opx1 | Opx2 | Opx3 | Opx4 |
| Li | 3.15 | 3.92 | 1.13 | 3.18 | bdl | 4.63 | 2.43 | 5.18 | 0.82 | 1.21 |
| Be | bdl | bdl | 0.06 | 0.01 | 0.04 | bdl | 0.13 | 0.03 | 0.16 | 0.12 |
| Cs | bdl | bdl | 0.07 | 0.02 | bdl | bdl | 0.19 | 0.05 | 0.12 | 0.08 |
| Rb | bdl | bdl | 0.18 | 0.06 | 0.20 | bdl | 0.41 | 0.09 | 0.29 | 0.14 |
| Ba | 0.04 | 0.03 | 1.32 | 1.95 | 1.85 | 0.12 | 0.51 | 1.68 | 2.76 | 0.66 |
| Pb | 0.06 | 0.01 | 0.06 | 1.27 | 0.27 | 0.01 | 0.07 | 0.18 | 0.87 | 0.02 |
| Th | bdl | bdl | 0.09 | 0.01 | 0.03 | bdl | 0.03 | 0.04 | 0.03 | 0.01 |
| U | bdl | bdl | 0.01 | 0.00 | 0.01 | bdl | 0.01 | 0.01 | 0.01 | 0.01 |
| Nb | 0.02 | 0.02 | 0.15 | 0.03 | 0.22 | 0.07 | 0.04 | 0.09 | 0.03 | 0.02 |
| Ta | bdl | bdl | 0.01 | bdl | bdl | 0.00 | 0.00 | 0.00 | 0.00 | 0.00 |
| P | 29.0 | 64.6 | 9.01 | 60.7 | 10.42 | 52.0 | 21.5 | 63.7 | 7.7 | 7.7 |
| La | 0.01 | 0.01 | 0.17 | 0.03 | 0.16 | 0.01 | 0.12 | 0.16 | 0.12 | 0.04 |
| Ce | 0.01 | 0.02 | 0.44 | 0.07 | 0.48 | 0.01 | 0.29 | 0.42 | 0.16 | 0.06 |
| Pr | bdl | 0.00 | 0.06 | 0.01 | 0.06 | 0.00 | 0.03 | 0.05 | 0.01 | 0.01 |
| Sr | 0.05 | 0.01 | 0.63 | 0.53 | 1.25 | 0.04 | 0.21 | 1.07 | 1.42 | 0.16 |
| Nd | bdl | 0.01 | 0.25 | 0.03 | 0.25 | bdl | 0.12 | 0.17 | 0.04 | 0.02 |
| Zr | 0.01 | bdl | 0.31 | 0.02 | 0.50 | 0.01 | 0.15 | 0.03 | 0.20 | 0.22 |
| Hf | bdl | bdl | bdl | bdl | bdl | bdl | 0.01 | bdl | 0.01 | 0.01 |
| Sm | bdl | bdl | 0.06 | bdl | 0.05 | bdl | 0.02 | 0.03 | 0.01 | 0.01 |
| Eu | bdl | bdl | 0.02 | 0.00 | 0.02 | bdl | 0.01 | 0.01 | 0.01 | 0.00 |
| Ti | 18 | 21 | 193 | 21 | 284 | 17 | 110 | 18 | 144 | 153 |
| Gd | bdl | bdl | 0.06 | 0.01 | 0.06 | bdl | 0.02 | 0.03 | 0.01 | 0.01 |
| Tb | bdl | bdl | 0.01 | bdl | 0.01 | bdl | 0.00 | 0.00 | 0.00 | bdl |
| Dy | bdl | bdl | 0.07 | 0.01 | 0.08 | bdl | 0.02 | 0.03 | 0.01 | 0.01 |
| Ho | bdl | bdl | 0.01 | 0.00 | 0.02 | bdl | 0.00 | 0.00 | 0.00 | 0.00 |
| Y | bdl | 0.02 | 0.36 | 0.03 | 0.54 | 0.00 | 0.12 | 0.10 | 0.08 | 0.05 |
| Er | bdl | bdl | 0.05 | 0.01 | 0.06 | bdl | 0.01 | 0.01 | 0.01 | 0.01 |
| Tm | bdl | bdl | 0.01 | bdl | 0.01 | bdl | 0.00 | 0.00 | 0.00 | 0.00 |
| Yb | bdl | bdl | 0.05 | 0.01 | 0.08 | bdl | 0.04 | 0.02 | 0.03 | 0.01 |
| Lu | bdl | bdl | 0.01 | 0.00 | 0.01 | bdl | 0.01 | 0.01 | 0.01 | 0.00 |
| Sc | 2.74 | 1.94 | 4.66 | 2.90 | 9.96 | 2.85 | 10.16 | 4.75 | 12.46 | 10.82 |

Trace element compositions of chlorite and olivine are expressed as averages. In brackets is the number of analyses included in the average. Mineral abbreviations as in Table 1. *bdl*=below detection limit.

$U_N > Th_N$, and a distinct positive anomaly for Pb (Fig. 7B). The HFSE elements display a negative anomaly with respect to REE of similar compatibility and there is a marked negative Li anomaly. Interestingly amphibole1 displays a negative Sr anomaly. Amphibole1 is more abundant in the more fertile samples (551, MR 136) but relics have been found also in the other samples. In sample 544, there is a gradual decrease in REE from hornblende (Amph 1) to tremolite (Amph 2). Tremolite in this sample and in MR 136 (Amph 2a in Fig. 7C-D) is characterised by much lower LILE contents and the disappearance of the positive Ba anomaly. $U_N$ is similar to $Th_N$ and there is a much smaller positive Pb anomaly. The negative Sr anomaly in tremolite has increased with respect to the hornblende. In sample MR207 tremolite (Amph 2b in Fig. 7C–D) displays similar features to what is observed in the other samples, apart from Pb that shows a negative anomaly. Also the negative Sr anomaly is most accentuated in this tremolite.

Further discrimination diagrams for the two amphibole types are presented in Fig. 8 and compared to amphibole data from garnet–amphibole peridotites reported by Scambelluri et al. (2006). On the basis of the (a) $Ba_N$ vs $Dy_N/Lu_N$ and (b) Sr vs Pb compositions it is clear that hornblende and tremolite plot in different fields. The pargasitic amphiboles from the garnet peridotites have high LILE content and the strongest HREE fractionation, the hornblende from spinel–amphibole peridotites has high LILE contents but no HREE fractionation whereas the tremolite displays the lowest LILE values. Therefore the change in metamorphic conditions from garnet–amphibole peridotites to amphibole-chlorite peridotites, which is documented in a change in major element composition of amphibole

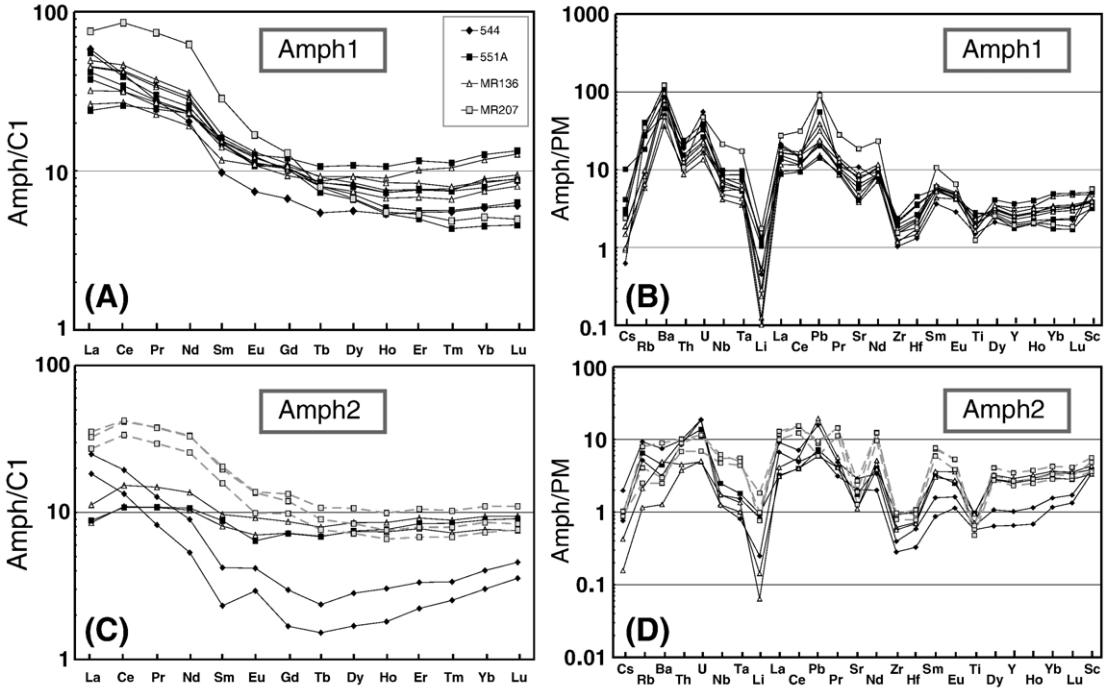


Fig. 7. Chondrite normalised REE and Primitive Mantle (PM) normalised trace element compositions of Amph 1(A–B) and Amph 2 (C–D). Solid lines in C–D refer to Amph 2a, dashed lines to Amph 2b. Description in text. Normalising values after Sun and McDonough (1989) for Chondrite and McDonough and Sun (1995) for PM.

(Fig. 6), is also mirrored in changing trace element characteristics of amphibole.

*Chlorite* contains very low concentrations of the investigated trace elements; nevertheless it features LREE enrichment and contains some large-ion-lithophile elements (Rb and Ba) as well as Li. Full REE and trace element compositions were measured for chlorites in samples 551A and MR136 and are presented in Fig. 9A–B. Chlorite displays a sub-chondritic REE pattern, characterised by weak LREE enrichment ($La_N/Gd_N = 1.35–2.88$) and rather flat HREEs ($Gd_N/Lu_N = 0.66–1.09$). LILE patterns in chlorite are similar to those of tremolite, but at much lower concentrations (Fig. 9B).

REE and trace element compositions have been measured for *orthopyroxene* in one of the samples (MR207). Orthopyroxene is characterised by a steep LREE pattern with decreasing contents with increasing atomic number and an opposite trend in HREE. All analyses display a positive Eu anomaly. LILE are all detectable in orthopyroxene and there are positive spikes in normalised Li and Pb abundances (Fig. 10A–B).

*Olivine* occurs as rare kinked porphyroclasts and as abundant small neoblasts arranged in granoblastic polygonal texture. Olivine has very low trace element contents (Table 5), except for some elements like Li and P. P

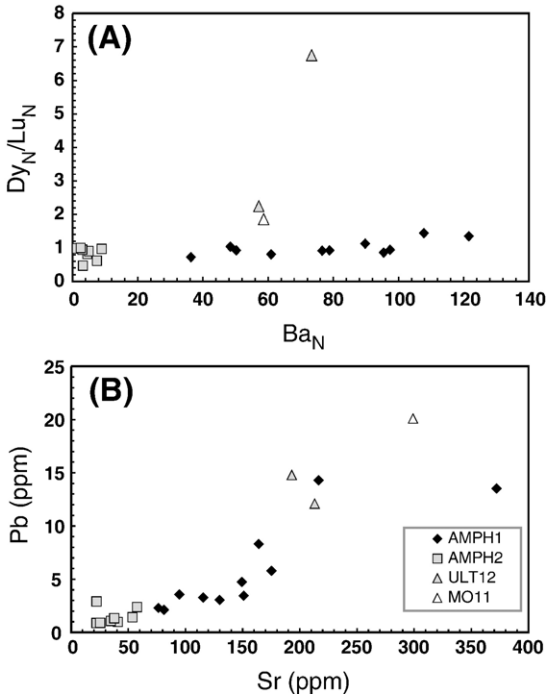


Fig. 8. Variability of trace elements in amphiboles: (A) $Ba_N$ vs $Dy_N/Lu_N$ and (B) Sr vs Pb. Compositions of ULT12 and MO11 from Scambelluri et al. (2006).

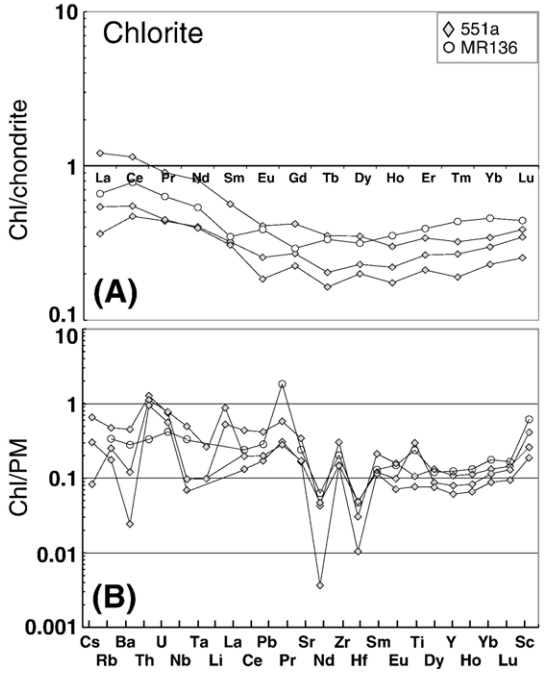


Fig. 9. Chondrite normalised REE (A) and Primitive Mantle (PM) normalised trace element (B) compositions of chlorite. Normalising values after Sun and McDonough (1989) for Chondrite and McDonough and Sun (1995) for PM.

and Li concentrations in olivine of all the analysed samples display a positive correlation. Therefore, we suggest a coupled substitution such as $^{[VI]}Mg^{2+}+{}^{[IV]}Si^{4+}=$ $^{[VI]}Li^{+}+{}^{[IV]}P^{5+}$ that could be responsible for the incorporation of Li in olivine. Our data is in agreement with Li data reported by Scambelluri et al. (2006) who observed that the lithium content in olivine progressively increases from Spl-lherzolites to Grt-peridotites to Chl-peridotites.

## 6. Discussion

### *6.1. Trace element constraints on the metamorphic evolution of chlorite peridotites*

Garnet and amphibole are commonly found in peridotites from the Ulten Zone (Obata and Morten, 1987; Rampone and Morten, 2001) and are known to coexist in Alpine-type peridotites from other localities, for example the Erzgebirge Crystalline Complex (Schmädicke and Evans, 1997). Previous studies (Morten and Trommsdorff, 2003; Morten et al., 2004) consider chlorite peridotites as the result of recrystallization and transformation of HT coarse spinel lherzolite via coarse HP garnet peridotite to fine-grained amphibole and chlorite–amphibole peridotites. This work outlines some textural and geochemical features that are not in agreement with this assumption.

In other studies, a high-pressure garnet peridotite stage has been proposed on the basis of garnet pseudomorphs, i.e. very fine-grained intergrowths of orthopyroxene, spinel and clinopyroxene and/or Al-bearing hornblende aggregates enclosing fine-grained spinel (Tsai et al., 2000). The association of tremolite and chlorite has also been observed in pseudomorphs after garnet in the lherzolite body from Cima di Gagnone (Evans and Trommsdorff, 1978), invoking re-equilibration under amphibolite facies conditions. The intergrowth of chlorite with Cr-rich spinel in the samples investigated in this study suggests that chlorite partly replaces former Al-rich spinel. Textural evidence of garnet is lacking in the chlorite–amphibole peridotites, such as chlorite pseudomorphs after garnet, pyroxene-spinel symplectite or aggregates of clinopyroxene + orthopyroxene + spinel. However, deformation might have obliterated such textures and hence additional evidence is needed to decide whether or not garnet was stable in these rocks.

Because garnet strongly fractionates REE, with preferential incorporation of HREE, the investigation of REE patterns of minerals assumed to have coexisted with garnet can be used as fingerprint for the presence or absence of garnet during the history of the rock. Amphiboles coexisting with garnet in the Ulten peridotites are

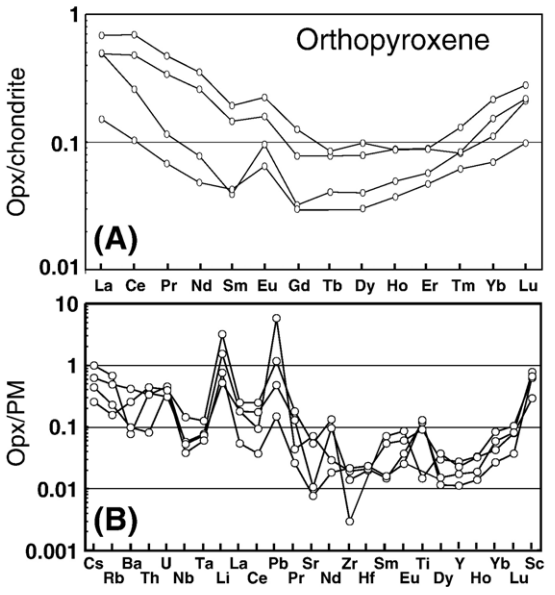


Fig. 10. Chondrite normalised REE (A) and Primitive Mantle (PM) normalised trace element (B) compositions of orthopyroxene. Normalising values after Sun and McDonough (1989) for Chondrite and McDonough and Sun (1995) for PM.

characterised by a steep HREE pattern with decreasing HREE contents with increasing atomic number and $Lu_N$ well below unity (Scambelluri et al., 2006). On the other hand amphiboles that replace garnet mimic the garnet trace element pattern and display increasing HREE contents with increasing atomic number (Scambelluri et al., 2006). This provides evidence that some spinel–amphibole peridotites derive from retrogressed garnet–amphibole peridotites. The flat or slightly enriched HREE character of all amphibole generations investigated in this study (Fig. 7) indicates that amphibole did neither equilibrate with nor grew at the expense of garnet. In particular, both geochemical signatures of the older hornblende (Amph1) (Fig. 7A–B) and orthopyroxene (Fig. 10), which can be assumed as stable phases in the precursor peridotite, do not point to coexistence with garnet. Also chlorite does not show any HREE enrichment and thus is unlikely to have replaced former garnet. The trace element data thus suggest that the relic minerals formed in the amphibole–spinel peridotite field whereas the main equilibration occurred in the chlorite–amphibole peridotite field.

There are two different hypotheses why garnet did not form in the investigated peridotites. 1) The rocks passed through the garnet peridotite field but for chemical or kinetic reasons no garnet formed. 2) The rocks never entered the garnet stability field. Chlorite peridotites cover the full compositional range of the Nonsberg peridotites in terms of major element compositions (Fig. 4). It is therefore unlikely that the apparent absence of garnet is related to a very depleted nature of the protolith. It is worth noting that some of the chlorite peridotites are among the most depleted peridotites of the Ulten Zone as also documented by the depletion in MREE and HREE. However, a significant portion of peridotites overlap in CaO, MgO and $Al_2O_3$ with samples that contain garnet (Fig. 4). It is therefore unlikely that bulk-rock composition could have prevented garnet formation. The activity of $H_2O$ is another parameter that needs consideration when the stability fields of garnet and chlorite peridotites are compared. Obata and Thompson (1981) showed that the assemblage Olivine + Orthopyroxene + Amphibole + Chlorite can be stable at high pressures provided that activity of $H_2O$ is high enough. However, a recent experimental study on the stability of chlorite peridotites under water saturated conditions (Fumagalli and Poli, 2005) showed that for the inferred peak pressure conditions of the Nonsberg peridotites ($T$ = 850 °C, $P \sim 2.7$ GPa) chlorite is not stable. The last alternative explanation is that some of the chlorite peridotites represent coarse-grained spinel peridotites that escaped garnet–amphibole formation due to the lack of fluids. Such spinel peridotites are extremely rare and no transitional stage between spinel peridotites and chlorite peridotites has been observed. In summary, we cannot find any justified argument that the lack of garnet is related to chemical reasons and therefore the presented data can better be explained with the second hypothesis, that the investigated rocks never entered the garnet stability field.

### *6.2. Metamorphic evolution and metasomatism recorded in amphiboles*

On the basis of textures, major and trace element compositions, two generations of amphibole can be distinguished. Major element compositional features of hornblende cores (Amph 1) are comparable to those of pargasitic hornblende from the Nonsberg fine-type peridotites (Obata and Morten, 1987) and of calcic amphiboles from a variety of alpine-type peridotites (Schmädicke and Evans, 1997). Amphibole in the Ulten chlorite peridotites is the most abundant metasomatic mineral and is the main host for trace elements. As such, amphibole can provide information about the origin and the timing of the metasomatic processes since its trace element composition is dependent on the nature and the trace-element composition of the agent which promoted its crystallization.

Fig. 11 shows the comparison of the average trace element pattern of amphiboles stable in the garnet field (Scambelluri et al., 2006) with the average trace element patterns of relic hornblende (Amph 1) that was stable in the spinel peridotite field, and tremolite (Amph 2), which formed during ongoing decompression.

In sample ULT12, representative of the eclogite-facies hydration, the HREE-depleted pattern indicates full equilibrium with garnet. The variable LILE-enriched character (Sr, Ba and Rb spikes) coupled with very low HFSE (Nb, Ta, Zr and Hf) concentrations in the Ulten amphiboles indicates that an aqueous fluid or a hydrous melt derived from subducted crustal rocks is the most likely metasomatic agent that infiltrated the cooled mantle wedge peridotites (Rampone and Morten, 2001; Scambelluri et al., 2006). The trace element pattern for the relic hornblende in the chlorite amphibole peridotites is very similar to the amphiboles from garnet–amphibole peridotites in terms of LREE and LILE enrichment. This observation implies that the fluids fluxing the garnet–amphibole and spinel–amphibole peridotites were sourced from a similar reservoir. A similar LILE-enriched, HFSE-depleted signature in amphibole has also been documented in peridotites from Finero and

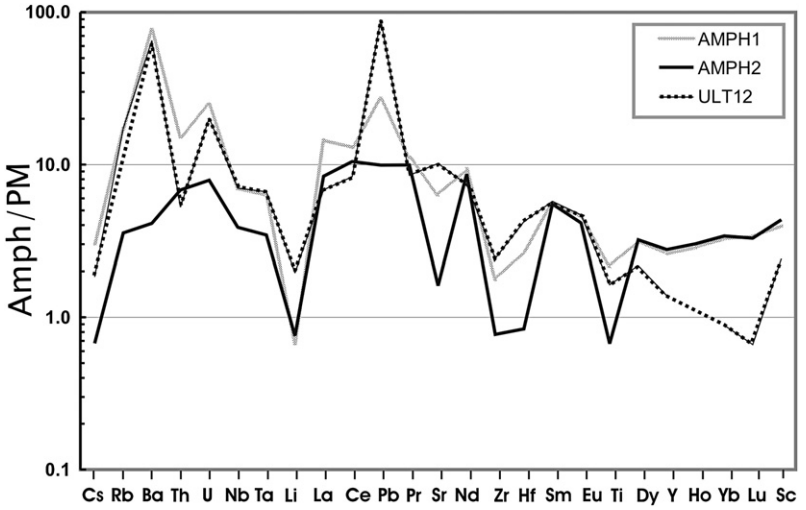


Fig. 11. Comparison of trace element patterns of amphiboles in chlorite peridotites (Amph 1–Amph 2) with amphibole from garnet–amphibole peridotite (ULT12), representative of the eclogite-facies hydration reported by Scambelluri et al. (2006).

interpreted as the product of metasomatism by hydrous melts (Zanetti et al., 1999), as well as in mantle xenoliths or mantle rocks contaminated by crustal-derived metasomatic agents (Dupuy et al., 1991; Piccardo et al., 1993). Nevertheless, there are some significant differences between amphibole from garnet–amphibole peridotites and spinel–amphibole peridotites. The hornblende (Amph 1) displays a negative Sr anomaly whereas ULT12 has a positive Sr anomaly (Fig. 11). Also the overall Sr and Pb content of the hornblende is smaller than what is observed in amphiboles that formed in coexistence with garnet (Fig. 8). The tremolite has significantly lower LILE and LREE contents than the hornblende. The positive Ba and Pb anomalies that are present in the hornblende disappear in the tremolite and the negative Sr anomaly increases. The observation that amphiboles with different trace element patterns occur within one sample indicates that the trace element characteristics are related to formation of the amphibole and are not affected by diffusion during later retrograde equilibration. ULT 12 formed at conditions of $T = 850$ °C, $P \sim 2.7$ GPa (Nimis and Morten, 2000), whereas the hornblende in the spinel-(chlorite)-amphibole peridotites likely formed at T ~ 750 °C, $P \leq 1.5$ GPa, and the tremolite in the chlorite–amphibole peridotites formed at $T =$ 650–700 °C, $P < 1.5$ GPa (Marocchi, 2006). Hence the observations provide evidence that the character of the fluid phase that metasomatised the peridotites changed with changing metamorphic conditions of the mantle wedge.

Using published amphibole-fluid partition coefficients the composition of the metasomatising fluid can be approximated. Brenan et al. (1995) determined fluid/amphibole partition coefficients for six elements at 900 °C, 2 GPa. The resulting fluid composition normalised to primitive mantle displays high values for fluid mobile elements such as Ba, Pb and U whereas Th, Nb and surprisingly Sr have much lower values (Fig. 12A). The fluid in equilibrium with tremolite has overall lower values and particularly the Ba/Th ratio is significantly different. It must be noted that the experimental temperature is significantly higher than what is expected for the formation of tremolite, and thus we have calculated a second set of fluid compositions at lower temperature. There is no direct experimental amphibole/fluid partitioning available for 700 °C. However, Green and Adam (2003) published clinopyroxene/fluid partitioning determined at 3 GPa and 700 °C in a basaltic composition. This partitioning can be combined with amphibole/clinopyroxene partitioning from a metasomatised mantle wedge peridotites given by Hermann et al. (2006b), which are very similar to the samples studied here, to obtain an amphibole/fluid partitioning. We have used the clinopyroxene I in run 1912 of Green and Adam (2003), which contains a comparable low jadeite component to the peridotitic clinopyroxene, and the average clinopyroxene and amphibole compositions of the first retrogression stage reported by Hermann et al. (2006b). Using this approach, the fluid composition for 12 elements has been calculated (Fig. 12B). The overall concentration of elements is significantly lower than what has been calculated using the Brenan et al. (1995) data. However, the pattern of the fluid composition is quite similar with positive spikes of

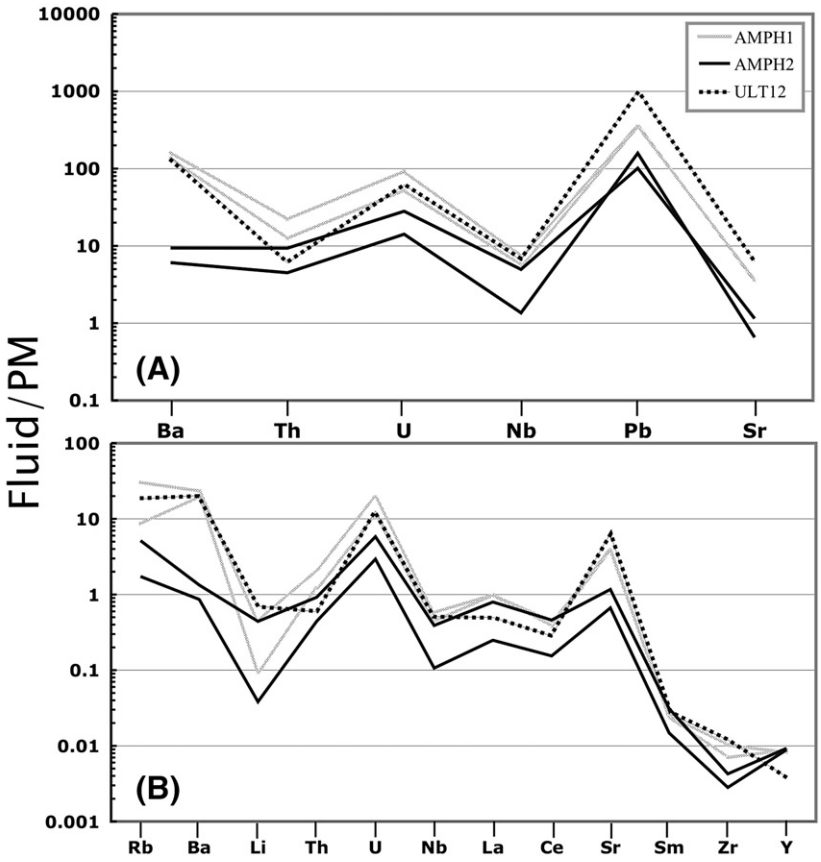


Fig. 12. Primitive Mantle (PM; McDonough and Sun, 1995) normalised trace element patterns of the estimated fluid calculated on the basis of amphibole-fluid partition coefficients from (A) Brenan et al. (1995) and (B) from a combination of clinopyroxene/fluid partitioning (Green and Adam, 2003) and amphibole/clinopyroxene partitioning (Hermann et al., 2006b). Amph 1 derive from averages from sample 551A and MR136, respectively; Amph 2 derive from averages from sample 544 and MR207, respectively.

fluid mobile elements. The most important difference is that Sr displays a positive anomaly with respect to LREE and Nb. The enriched LILE signature provides strong evidence that the fluid is sourced from subducted continental crust. The decrease in Sr and the decreasing Sr anomaly in the fluid concomitant with the cooling and decompression of the mantle wedge peridotites could be explained with the appearance of plagioclase as a stable phase in the subducted crust from where the fluid is sourced. Another observation is that the fluid composition in equilibrium with tremolite (Amph 2), which formed at relatively lower pressure and temperature, is much more dilute than the fluid in equilibrium with the higher-grade amphiboles (Amph 1 and ULT12). At the approximate *P-T* conditions where the tremolite–chlorite peridotites formed, it is likely that a diluted aqueous fluid is stable in the associated subducted crustal rocks (Hermann et al., 2006a). In contrast, at metamorphic conditions similar to what the amphibole–spinel peridotite and garnet peridotite experienced, the fluid phase in equilibrium with the subducted crust is likely a hydrous felsic melt (Hermann et al., 2006a). Such a hydrous felsic melt could directly react with the mantle wedge peridotites to form trace element-rich amphibole as experimentally demonstrated by Rapp et al. (2006). Alternatively, the melt might react with peridotites to form garnet-orthopyroxenites at the slab-mantle interface and a residual trace element rich aqueous fluid that is able to metasomatise more internal parts of the mantle wedge (Malaspina et al., 2006). In any case the observed evolution from garnet–amphibole to spinel–amphibole to chlorite–tremolite peridotite provides evidence that the metasomatising fluid is getting more diluted during exhumation of the mantle wedge peridotites.

The occurrence of dolomite as metasomatic minerals, reported in the Ulten peridotites by Obata and Morten (1987), suggests that the metasomatic fluids must also

have had a $CO_2$ component (Rampone and Morten, 2001). Equilibrium temperatures calculated with THERMOCALC (Powell and Holland, 1988) for chlorite peridotites vary from 650° to 780 °C, for $aH_2O$ 0.4–0.7 (Marocchi, 2006). Estimated temperatures and the $aH_2O$ range are consistent with the nature of the fluid as a $H_2O$-fluid containing other volatile components, among which $CO_2$ is likely to occur.

### 6.3. Origin of positive Eu-anomaly

The Group 1 peridotites (Fig. 5), which show significant depletion because of low HREE contents, are characterised by a strong enrichment in LREE and particularly by a positive Eu anomaly. This type of REE pattern has not been previously reported for the Ulten peridotite (Fig. 4A) and its origin remains enigmatic. The detailed mineral trace element study of the transition from anhydrous hot spinel peridotites to cool hydrous garnet–amphibole peridotites by Scambelluri et al. (2006) revealed that there are two distinct stages of metasomatism recorded in the Ulten peridotites. There is a "hot" metasomatism caused by interaction of peridotites with melt that led to a pronounced LREE enrichment of the rocks followed by a "cold" metasomatism by aqueous fluids sourced from subducted crust as discussed above. In the investigated samples there is also evidence that the observed enrichment in LREE and the positive Eu anomaly in bulk rock and minerals are related to an earlier metasomatic event. The trace element signature of orthopyroxene relics displays flat Th–U indicating that they formed prior to the subduction related metasomatism. The REE patterns of orthopyroxene in this sample are strongly LREE-enriched and display a positive Eu anomaly. This indicates that the LREE and Eu enrichment are the results of interaction with a LREE-enriched agent, most likely a melt phase. We suggest that the protoliths of such chlorite peridotites could have been mantle rocks metasomatised by melts at low pressures in the plagioclase stability field, and the positive Eu anomaly originates from crystallized plagioclase (e.g. Müntener et al., 2004). Retrogressed garnet peridotites from the Eastern Alps are characterised by significant positive Eu anomalies (Janák et al., 2006). Incompatible elements and REE patterns of these peridotites are comparable to those of the Nonsberg chlorite peridotites, but the latter are quite different in other respects, i.e. lower $Al_2O_3$, CaO, higher MgO contents and higher LREE and LILE enrichment. The timing of this pristine metasomatic event, leading to the strong enrichment in LREE and the positive Eu-anomaly in the investigated chlorite peridotites, is unconstrained and could be related to a pre-Variscan event.

### 6.4. Implications on entrapment of peridotites within the crust

It is generally assumed that mantle wedge peridotites, which now occur as lenses within gneisses, have been entrapped at peak metamorphic conditions within subducted continental crust and then were brought back to the surface together (Brueckner, 1998; Brueckner and Medaris, 2000; Brueckner and Van Roermund, 2004). Similar ages for the peridotites and country rock gneisses led Tumiati et al. (2003) to conclude that this is also the case for the Ulten Peridotite. Also, Rampone and Morten (2001) suggested that the LILE enrichment observed in garnet–amphibole peridotites occurred during incorporation of the peridotites into the crust. This interpretation was not fully supported by the recent findings of Scambelluri et al. (2006), who noted that the absence of any pyroxenite rind around the peridotite body is inconsistent with peridotite–gneiss interaction at the conditions recorded in the garnet amphibole peridotite (800 °C, 3.0 GPa). Instead, Scambelluri et al. (2006) suggested that the incorporation of peridotite lenses into the crust occurred during exhumation. Models by Ranalli et al. (2005) claim that exhumation and cooling of the garnet peridotites was due to extrusion of the Ulten slice along the subduction channel during continuing subduction and consisted of two exhumation stages. A first fast exhumation stage, as observed in Alpine UHP crustal rocks (Rubatto and Hermann, 2001), driven by the upward buoyancy of crustal material, was followed by a slow stage related to slab break-off with consequent lithospheric extension. The model favours entrainment of the peridotites into the crust at peak metamorphic conditions but does not account for any further incorporation of mantle rocks slices during exhumation.

Our new data put additional constraints on the incorporation of peridotites into the crust. Textures and trace elements of minerals in chlorite–amphibole peridotites investigated in this study provide evidence that these rocks never equilibrated in the garnet peridotite field. This observation suggests that at least some of the peridotite lenses were incorporated into the crust during exhumation. This hypothesis is in agreement with the metasomatic history of the peridotites as documented in the amphiboles. The changing pattern of pargasite in garnet peridotites to pargasite–hornblende in spinel peridotites to tremolite in chlorite peridotites indicates that decompression of the mantle rocks took place within the mantle wedge where the rocks interacted with crustal-derived fluids during exhumation. A relatively late incorporation into the crust is supported by the comparison of the *P-T* path of gneisses and

mantle rocks. Braga et al. (2006) have recently proposed a clockwise *P-T* path for the Ulten Zone metapelitic gneisses, characterised by a near isobaric heating stage, which led to dehydration melting of white mica responsible for the origin of migmatites, followed by a nearly isothermal decompression representing exhumation. Such a *P-T* evolution may be related to subduction of continental crust as suggested by Nimis and Morten (2000). However the range of pressure estimates by Braga et al. (2006), i.e. 1.2–1.5 GPa at 520 °C and 1.0–1.4 GPa at the peak T of 565–715 °C, contrasts with the very high pressure (≈2.7 GPa) prograde path inferred by Tumiati et al. (2003). On the basis of pressures estimated using inclusion in kyanite and garnet, the metapelites appear to share the same decompressional *P-T* path of chlorite peridotites starting from 1.2–1.4 GPa. The new findings indicate that slices of crust originating from different crustal levels and mantle rock slices with different *P-T* trajectories have been tectonically assembled within the Ulten Zone during exhumation.

## 7. Summary and conclusions

In situ trace element analysis of hydrous phases is a powerful tool to unravel different stages of metasomatism within peridotites. Chlorite–amphibole peridotites exhibit various degrees of metasomatic enrichment as indicated by the trace element patterns of amphiboles and by bulk-rock trace-element patterns. The observed trace-element patterns are consistent with metasomatism by different agents or combination of agents, which have acted at different stages. We propose that the earliest stage represents impregnation of peridotites by a hydrous melt unrelated to subduction. This metasomatic event produced LREE enrichment and, in some samples, a positive Eu anomaly in bulk rocks. This metasomatic imprint is preserved in porphyroclastic orthopyroxene relics. The metasomatism leading to spinel–amphibole peridotites and chlorite–amphibole peridotites is related to the progressive influx of a hydrous fluid with crustal signature derived from neighbouring subducted continental crust. The trace element characteristics of early formed hornblende in spinel–amphibole peridotites indicate that the metasomatic agent contained high amounts of fluid-mobile elements whereas tremolite in the chlorite–amphibole peridotites formed from a diluted aqueous fluid. Amphiboles formed during these metasomatic stages display LILE enrichment but have flat HREE patterns indicating that they never equilibrated with garnet. Chlorite does not display any HREE enrichment as is the case when chlorite forms pseudomorphs after garnet. Additionally, the textures suggest that chlorite originates from former Al-rich spinel. These observations suggest that the investigated chlorite peridotites don't represent retrogressed garnet peridotites, but derive from spinel peridotites that never equilibrated in the garnet stability field. The observation that garnet peridotites and chlorite peridotites are hosted within the same gneisses indicates that slices of mantle wedge peridotite with different *P-T* trajectories have been sampled by subducted crust.

## Acknowledgements

The analyses were performed by M.M. during a stage at the Research School of Earth Sciences, The Australian National University, Canberra. Dr. Nicola Sasanelli, the Scientific Attaché of the Italian Embassy in Canberra, and the Australian National University are kindly acknowledged for financial support and warm hospitality. R. Carampin (CNR-IGG Padova) is thanked for assistance during EMPA analyses. Journal reviews by S. Klemme and M. Obata and editorial comments by O. Müntener helped to improve the paper. M.M is thankful to R. Braga for personal comments and discussion. G.M. Bargossi and V. Mair (Autonomous Provinz Bozen) are kindly acknowledged for help with field work. Additional support was provided by the Italian MIUR-COFIN 2003 (project "Mass-transfer and role of fluids during peridotite emplacement in subducting continental crust: natural and experimental constraints") and MIUR-COFIN 2005 (project "C–O–H fluids, hydrates, carbonates and crust–mantle mass transfer in subduction zones") to L.M. J.H acknowledges financial support from the Australian Research Council.

## References

Bodinier, J.-L., Godard, M., 2004. Orogenic, ophiolitic and abyssal peridotites. In: Holland, H.D., Turrekian, K.K. (Eds.), Treatise on Geochemistry. Elsevier, Amsterdam, pp. 103–170.

Braga, R., Massonne, H.-J., Morten, L., 2006. Constraining the prograde *P-T* path using mineral inclusions in kyanite and garnet: an example from metapelites of the Ulten Zone gneiss (Northern Italy). Geophys. Res. Abstr. 8, 02985.

Brenan, J.M., Shaw, F.F., Ryerson, F.J., Phinney, D.L., 1995. Mineral-aqueous fluid partitioning of trace elements at 900 °C and 2.0 GPa: constraints on the trace element chemistry of mantle and deep crustal fluids. Geochim. Cosmochim. Acta 59, 3331–3350.

Brueckner, H.K., 1998. Sinking intrusion model for the emplacement of garnet-bearing peridotites into continent collision orogens. Geology 26 (7), 631–634.

Brueckner, H.K., Medaris, L.G., 2000. A general model for the intrusion and evolution of "mantle" garnet peridotites in high-pressure and ultra-high-pressure metamorphic terranes. J. Metamorph. Geol. 18, 123–133.

Brueckner, H.K., Van Roermund, H.L.M., 2004. Dunk Tectonics: a multiple subduction/eduction model for the evolution of the Scandinavian Caledonides. Tectonics 23, 1–20.

Buick, I.S., Hermann, J., Williams, I.S., Gibson, R.L., Rubatto, D., 2006. A SHRIMP U–Pb and LA-ICP-MS trace element study of the petrogenesis of garnet-cordierite-orthoamphibole gneisses from the Central Zone of the Limpopo Belt, South Africa. Lithos 88, 150–172.

Dupuy, C., Mevel, C., Bodinier, J.L., Savoyant, L., 1991. Zabargad peridotite: evidence for multistage metasomatism during Red Sea rifting. Geology 19, 722–725.

Evans, B.W., Trommsdorff, V., 1978. Petrogenesis of garnet lherzolite, Cima di Gagnone, Lepontine Alps. Earth Planet. Sci. Lett. 40, 333–348.

Fumagalli, P., Poli, S., 2005. Experimentally determined phase relations in hydrous peridotites to 6.5 GPa and their consequences on the dynamics of subduction zones. J. Petrol. 46, 555–578.

Godard, G., Martin, S., Prosser, G., Kienast, J.R., Morten, L., 1996. Variscan migmatites, eclogites and garnet–peridotites of the Ulten Zone, Eastern Austroalpine system. Tectonophysics 259, 313–341.

Green, T.H., Adam, J., 2003. Experimentally-determined trace element characteristics of aqueous fluid from dehydrated mafic oceanic crust at 3.0 GPa, 650–700 °C. Eur. J. Mineral. 15, 815–830.

Hermann, J., Spandler, C., Hack, A., Korsakov, A.V., 2006a. Aqueous fluids and hydrous melts in high-pressure and ultra-high pressure rocks: implications for element transfer in subduction zones. Lithos 92, 399–417.

Hermann, J., Rubatto, D., Trommsdorff, V., 2006b. Sub-solidus Oligocene zircon formation in garnet peridotite during fast decompression and fluid infiltration (Duria, Central Alps). Mineral. Petrol. 88, 181–206.

Janák, M., Froizheim, N., Vrabec, M., Krogh Ravna, E.J., De Hoog, J.C.M., 2006. Ultrahigh-pressure metamorphism and exhumation of garnet peridotite in Pohorje, Eastern Alps. J. Metamorph. Geol. 24, 19–31.

Klemme, S., O'Neill, H.St.C., 2000. The near-solidus transition from garnet lherzolite to spinel lherzolite. Contrib. Mineral. Petrol. 138, 237–248.

Kretz, R., 1983. Symbols for rock-forming minerals. Am. Mineral. 68, 277–279.

Leake, B.E., Woolley, A.R., Arps, C.E.S., Birch, W.D., Gilbert, M.C., Grice, J.D., Hawthorne, F.C., Kato, A., Kisch, H.J., Krivovichev, V.G., Linthout, K., Laird, J., Mandarino, J.A., Maresch, W.V., Nickel, E.H., Rock, N.M.S., Schumacher, J.C., Smith, D.C., Stephenson, N.C.N., Ungaretti, L., Whittaker, E.J.W., Youzhi, G., 1997. Nomenclature of amphiboles: report of the subcommittee on amphiboles of the international mineralogical association, commission on new minerals and mineral names. Mineral. Mag. 61, 295–321.

Malaspina, N., Hermann, J., Scambelluri, M., Compagnoni, R., 2006. Polyphase inclusions in garnet–orthopyroxenite (Dabie Shan, China) as monitors for metasomatism and fluid-related trace element transfer in subduction zone peridotite. Earth Planet. Sci. Lett. 249, 173–187.

Marocchi, M., 2006. Petrological and geochemical characterization of chlorite–peridotites from the Ulten Zone (Nonsberg-Ultental, Italy): implications on the metasomatic processes. Unp. Ph.D. Thesis, Università di Bologna, Italy, 150 pp.

Marocchi, M., Bargossi, G.M., Braga, R., Morten, L., 2005. Mantle wedge-fluids interactions during the Variscan subduction: the case of chlorite peridotites from the Ulten Zone, Italy. European Geosciences Union 2005. Geophys. Res. Abstr. 7, 02136.

McDonough, W.F., Sun, S.-S., 1995. The composition of the Earth. Chem. Geol. 120, 223–253.

Morten, L., 1993. Ultramafic rocks in the Eastern Alps. In: Morten, L. (Ed.), Italian Eclogites and Related Rocks. Accademia Nazionale delle Scienze, Scritti e Documenti XIII, Roma.

Morten, L., Obata, M., 1990. Rare earth abundances in the Eastern Alpine peridotites, Nonsberg area, Northern Italy. Eur. J. Mineral. 2, 643–653.

Morten, L., Trommsdorff, V., 2003. Metamorphism and textures of dry and hydrous garnet peridotites. In: Carswell, D.A., Compagnoni, R. (Eds.), Ultrahigh pressure metamorphism, vol. 5. Eotvos University Press, Budapest, pp. 443–466 (Hungary).

Morten, L., Bargossi, G.M., Landini Bargossi, F., 1976. Notizie preliminari sulle metamorfiti della Val di Rumo, Val di Non, Trento. Mineral. Petrogr. Acta 21, 137–144.

Morten, L., Nimis, P., Rampone, E., 2004. Records of mantle–crust exchange processes during continental subduction–exhumation in the Nonsberg-Ultental garnet peridotites (eastern Alps). A review. Period. Mineral. (ISSN: 0369-8963) 73, 119–129 (Special issue 2).

Müntener, O., Pettke, T., Desmurs, L., Meier, M., Schaltegger, U., 2004. Refertilization of mantle peridotite in embryonic ocean basins: trace element and Nd isotopic evidence and implications for crust–mantle relationships. Earth Planet. Sci. Lett. 221, 293–308.

Nimis, P., Morten, L., 2000. *P-T* evolution of 'crustal' garnet peridotites and included pyroxenites from Nonsberg area (upper Austroalpine), NE Italy: from the wedge to the slab. J. Geodyn. 30, 93–115.

Obata, M., Morten, L., 1987. Transformation of spinel lherzolite to garnet lherzolite in ultramafic lenses of the Austridic crystalline Complex, Northern Italy. J. Petrol. 28, 599–623.

Obata, M., Thompson, A.B., 1981. Amphibole and chlorite in mafic and ultramafic rocksin the lower crust and upper mantle. Contrib. Mineral. Petrol. 77, 74–81.

O'Neill, H.St.C., 1981. The transition between spinel lherzolite and garnet lherzolite, and its use as a geobarometer. Contrib. Mineral. Petrol. 77, 185–194.

Pearce, N.J.G., Perkins, W.T., Westgate, J.A., Gorton, M.P., Jackson, S.E., Neal, C.R., Chenery, S.P., 1997. A compilation of new and published major and trace element data for NIST SRM 610 and NIST SRM 612 glass reference materials. Geostand. Newsl. 21, 115–144.

Piccardo, G.B., Rampone, E., Vannucci, R., Shimizu, W., Ottolini, L., Bottazzi, P., 1993. Mantle processes in the sub-continental lithosphere: the case study of the rifted sp-lherzolites from Zabargad (Red Sea). Eur. J. Mineral. 5, 1039–1056.

Pouchou, J.L., Pichoir, F., 1984. A new model for quantitative x-ray microanalysis. Part 1: application to the analysis of homogeneous samples. La Recherche Aérospatiale no. 3, pp. 167–192.

Powell, R., Holland, T.J.B., 1988. An internally consistent dataset with uncertainties and correlations: 3. Applications to geobarometry, worked examples and a computer program. J. Metamorph. Geol. 6, 173–204.

Rampone, E., Morten, L., 2001. Records of crustal metasomatism in the garnet peridotites of the Ulten Zone (Upper Austroalpine, Eastern Alps. J. Petrol. 42, 207–219.

Ranalli, G., Martin, S., Mahatsente, R., 2005. Continental subduction and exhumation: an example from the Ulten Unit, Tonale Nappe, Eastern Austroalpine. In: Gapais, D., Brun, J.P., Cobbold, P.R. (Eds.), Deformation Mechanisms, Rheology and Tectonics: From Minerals to the Lithosphere. Geol. Soc. Lond. Spec. Pub., vol. 243, pp. 159–174.

Rapp, R.P., Laporte, D., Martin, H., Shimizu, N., 2006. Experimental insights into slab–mantle interactions in subduction zones: melting of adakite-metasomatized peridotite and the origin of the "arc signature". Geochim. Cosmochim. Acta 70, A517.

Robinson, J.A.C., Wood, B.J., 1998. The depth of the spinel to garnet transition at the peridotite solidus. Earth Planet. Sci. Lett. 164, 277–284.

Rubatto, D., Hermann, J., 2001. Exhumation as fast as subduction? Geology 29, 3–6.

Scambelluri, M., Hermann, J., Morten, L., Rampone, E., 2006. Melt-versus fluid-induced metasomatism in spinel to garnet wedge peridotites (Ulten Zone, Eastern Italian Alps): clues from trace element and Li abundances. Contrib. Mineral. Petrol. 151, 372–394.

Schmädicke, E., Evans, B.W., 1997. Garnet-bearing ultramafic rocks from the Erzgebirge, and their relation to other settings in the Bohemian Massif. Contrib. Mineral. Petrol. 127, 57–74.

Sun, S.-S., McDonough, W.F., 1989. Chemical and isotopic systematics of oceanic basalts: implications for mantle composition and processes. In: Saunders, A.D., Norry, M.J. (Eds.), Magmatism in the Ocean Basins. Geol. Soc. Lond. Spec. Pub., vol. 42, pp. 313–345.

Trommsdorff, V., Hermann, J., Müntener, O., Pfiffner, M., Risold, A.C., 2000. Geodynamic cycles of subcontinental lithosphere in the Central Alps and the Arami enigma. J. Geodyn. 30, 77–92.

Tsai, C.H., Liou, J.G., Ernst, W.G., 2000. Petrological characterization and tectonic significance of retrogressed garnet peridotites, Raobazhai area, North Dabie Complex, east-central China. J. Metamorph. Geol. 18, 181–192.

Tumiati, S., Thöni, M., Nimis, P., Martin, S., Mair, V., 2003. Mantle–crust interactions during Variscan subduction in the Eastern Alps (Nonsberg-Ulten Zone): geochronology and new petrological constraints. Earth Planet. Sci. Lett. 210, 509–526.

Workman, R.K., Hart, S.R., 2005. Major and trace element compositions of the depleted MORB mantle (DMM). Earth Planet. Sci. Lett. 231, 53–72.

Zanetti, A., Mazzucchelli, M., Rivalenti, G., Vannucci, R., 1999. The Finero phlogopite peridotite massif: an example of subduction-related metasomatism. Contrib. Mineral. Petrol. 134, 107–122.